NASA TECHNICAL NOTE

NASA TN D-8239

NASA TN D-8239

AN ENGINEERING PROCEDURE FOR CALCULATING COMPRESSIVE STRENGTH OF ISOGRID CYLINDRICAL SHELLS WITH BUCKLED SKIN

Walter L. Heard, Jr., Melvin S. Anderson, and Paul Slysh

Langley Research Center
Hampton, Va. 23665

NATIONAL AERONAUTICS AND SPACE ADMINISTRATION • WASHINGTON, D. C. • JUNE 1976

AN ENGINEERING PROCEDURE FOR CALCULATING COMPRESSIVE STRENGTH OF ISOGRID CYLINDRICAL SHELLS WITH BUCKLED SKIN

Walter L. Heard, Jr., Melvin S. Anderson, and Paul Slysh*
Langley Research Center

SUMMARY

An engineering procedure is presented for calculating the compressive buckling strength of isogrid cylinders using shell-of-revolution techniques and accounting for loading beyond the material proportional limit and/or local buckling of the skin prior to general buckling. A general nondimensional chart (based on a nonlinear postbuckling analysis of a typical skin element) is presented which can be used in conjunction with formulas based on simple deformation plasticity theory to calculate postbuckling stiffnesses of the skin. The stiffening grid system is treated as an equivalent isotropic grid layer. Stiffnesses are determined for this grid layer, when loaded beyond the proportional limit, by the same plasticity theory used for the skin and a nonlinear stress-strain curve constructed from simple isogrid-handbook formulas and standard-reference-manual stress-strain curves for the material involved. Comparison of prebuckling strains and buckling results obtained by this procedure with data from a large isogrid-cylinder test is excellent with the calculated buckling load no more than 4 percent greater than the test value.

INTRODUCTION

The isogrid concept for stiffened structure has been found to be efficient and practical in such aerospace structures as launch-vehicle nose fairings, adapters, cylindrical sections of propellant tanks, and in Skylab floor and wall panels. Isogrid structure has high-strength/mass-ratio potential and, with modern machining capabilities may see widespread use in future aerospace applications. As indicated in reference 1, isogrid panels machined from solid-plate material can be an economical alternative to conventional skin-stringer construction as well as a more efficient structure. An engineering procedure is presented herein for calculating the compressive buckling strength of isogrid cylinders using shell-of-revolution techniques and accounting for loading beyond the material proportional limit and/or local buckling of the skin prior to general buckling. The term "isogrid" is used here in the usual sense, which implies that the cylinder wall is made up of a thin skin with integral stiffening members (see ref. 2) that form a network

*General Dynamics Corporation, Convair Division, San Diego, California.

of equilateral triangles. The stiffening grid acts as an isotropic material; thus, the grid properties can be averaged to form an equivalent-stiffness isotropic layer. For some designs, however, the skin buckles at relatively low loading compared to the maximum load-carrying capability of the cylinder; thus, the postbuckling stiffness properties of the skin must be taken into account for accurate analysis. This paper will present general results in the form of charts which can be used for determining such postbuckling skin-stiffness properties.

In order to demonstrate the applicability of this analysis procedure, a large isogrid cylinder which was previously tested (refs. 3 and 4) to buckling failure under axial and bending loads is analyzed. The test result is reported in reference 3 to be 48 percent of that predicted from a simple, general instability analysis using elastic material properties and effective skin width. Since the primary utility of such a test is to establish the accuracy of analytical methods, however, a more refined analysis was performed which takes into account structural behavior that cannot be handled in simplified analyses. Thus, the effectiveness of shell-of-revolution analysis is shown herein by accounting for such details as boundary conditions, asymmetric loading, prebuckling stresses and deformations, plasticity, buckled skin, and initial imperfections. All of the aforementioned structural aspects are examined in the present paper in order to gain insight into the discrepancy between the simple theory and the test results reported in reference 3.

SYMBOLS

A	cross-sectional area of typical stiffening grid member
B	stiffness parameter (see eq. (9))
E	elastic modulus of material
E_{eq}	equivalent modulus of stiffening grid layer
E_{sec}	secant modulus
E_{tan}	tangent modulus
E_x, E_y	extensional stiffnesses in x- and y-direction, respectively (see eqs. (4) and (5))
G_{xy}	inplane shear stiffness (see eq. (6))

g	factor related to onset of plasticity (see eqs. (15))
h	altitude of typical equilateral triangle formed by stiffening grid members
I	cross-sectional moment of inertia of typical stiffener in isogrid
K_μ	plasticity factor defined by equation (13)
M	applied bending moment
N_x,N_y	inplane stress resultants in axial and transverse directions, respectively
$N_{x,exp}$	buckling value of axial inplane stress resultant determined from experiment
n	number of circumferential waves for buckling
P	applied axial load through geometric center of cylinder cross section
R	radius of cylinder
s	axial coordinate with origin at cylinder midlength
t	skin thickness
t_{eq}	thickness of equivalent stiffening grid layer
u,v,w	displacements in x, y, and normal directions, respectively
w_i	assumed initial imperfection of model for Structural Analysis of General Shells (STAGS) nonlinear analysis (see eq. (17))
w_o	measured initial imperfection of test cylinder
Δw_o	peak deviation of measured initial imperfection from average value
x,y	axial and circumferential coordinates, respectively
$\alpha\beta_x,\alpha\beta_y,\alpha\beta_{xy}$	plasticity factors defined by equations (10), (11), and (12), respectively
ϵ	strain

ϵ_{cr} local buckling strain for equilateral triangular plate

ϵ_{eq} strain for equivalent stiffening grid layer

ϵ_x, ϵ_y strains in axial and circumferential directions, respectively

$\epsilon_{x,cr}, \epsilon_{y,cr}$ strains in x- and y-directions, respectively, at skin local buckling load

θ circumferential coordinate of cylinder

μ Poisson's ratio

μ_e elastic value of Poisson's ratio

μ_{eq} Poisson's ratio for equivalent stiffening grid layer

μ_x, μ_y Poisson's ratio associated with bending in x- and y-direction, respectively

σ stress

σ_{cr} local buckling stress for equilateral triangular plate

σ_{eq} stress for equivalent stiffening grid layer

ANALYSIS PROCEDURE

The general approach is a shell-of-revolution analysis with special treatment given to account for the stiffening grid structure, plasticity effects, and buckled skin.

Shell-of-Revolution Model

In the analysis procedure used herein the shell is modeled as an axisymmetric structure. The Structures Research Associates (SRA) shell-of-revolution computer code (refs. 5 and 6) is used for the analysis procedure, although several other codes of similar capability are available (see, for example, refs. 7 and 8) and could be used. The modeling entails replacing the actual wall section such as that shown in detail A-A of figure 1 with the equivalent two-layer shell wall shown to the right. As indicated, the stiffening grid is replaced by an equivalent-stiffness isotropic layer whose midplane is maintained at the same location as the center of gravity of a typical stiffening member. Likewise, the skin midplane location is maintained. In general, these two layers will not be

contiguous; thus, in computer programs that process layer properties to yield shell-wall bending stiffnesses it is convenient to introduce a third layer of zero stiffness. The function of this "fictitious" layer is simply to act as a spacer to fill the gap between the two layers of the equivalent shell wall shown in figure 1. Introducing this third layer will assure that representative stiffnesses of the isogrid wall including bending-coupling effects are achieved.

Calculation of Layer Properties

Elastic properties of stiffening grid.- The elastic isotropic properties of the equivalent stiffening grid layer are determined from the equations of reference 2, which can be written in the following form:

$$E_{eq} = \frac{EA^{3/2}}{2h\sqrt{3I}} \tag{1}$$

$$t_{eq} = 2\sqrt{\frac{3I}{A}} \tag{2}$$

$$\mu_{eq} = \frac{1}{3} \tag{3}$$

where E_{eq} is the equivalent modulus of elasticity, t_{eq} is the equivalent thickness, and μ_{eq} is the equivalent Poisson's ratio. In these expressions, E is the elastic modulus of the material, A is the cross-sectional area of a typical stiffening grid member, and I is its moment of inertia. The quantity h in equation (1) is the altitude of a typical equilateral triangle formed by intersections of the stiffening grid members (see fig. 1).

Equivalent orthotropic constants for plastic deformations.- In cases where the buckling strain is greater than the proportional-limit strain of the material, the buckling load can be calculated by making use of the equations for orthotropic shell-wall stiffnesses based on deformation plasticity theory developed and presented in reference 9. These equations are also used herein to calculate the postbuckling stiffness of the isogrid skin by assuming that the buckled skin acts as an isotropic plate strained beyond the proportional limit. The expressions for the orthotropic stiffnesses are:

$$E_x = B\left(1 - \mu_x\mu_y\right)\left(1 - \alpha\beta_x\right) \tag{4}$$

$$E_y = B\left(1 - \mu_x\mu_y\right)\left(1 - \alpha\beta_y\right) \tag{5}$$

$$G_{xy} = \frac{B(1 - \mu)}{2} \tag{6}$$

$$\mu_x = \mu\left(\frac{1 - \alpha\beta_{xy}}{1 - \alpha\beta_y}\right) \tag{7}$$

$$\mu_y = \mu\left(\frac{1 - \alpha\beta_{xy}}{1 - \alpha\beta_x}\right) \tag{8}$$

where, for uniaxial stress,

$$B = \frac{E_{sec}t}{1 - \mu^2} \tag{9}$$

$$\alpha\beta_x = \frac{(2 - \mu)^2}{4(1 - \mu^2)}\left(\frac{1 - \frac{E_{tan}}{E_{sec}}}{K_\mu}\right) \tag{10}$$

$$\alpha\beta_y = \frac{(1 - 2\mu)^2}{4(1 - \mu^2)}\left(\frac{1 - \frac{E_{tan}}{E_{sec}}}{K_\mu}\right) \tag{11}$$

$$\alpha\beta_{xy} = -\frac{(2 - \mu)(1 - 2\mu)}{4\mu(1 - \mu^2)}\left(\frac{1 - \frac{E_{tan}}{E_{sec}}}{K_\mu}\right) \tag{12}$$

$$K_\mu = 1 - \frac{(1 - 2\mu)\left(1 - \frac{E_{tan}}{E_{sec}}\right)}{2(1 - \mu^2)}\left[2\mu - \frac{1}{2}(1 + 2\mu)\right] \tag{13}$$

$$\mu = \frac{1}{2} - \left(\frac{1}{2} - \mu_e\right)\frac{E_{sec}}{E} \tag{14}$$

In the preceding expressions E_x and E_y are the extensional stiffnesses in the longitudinal and circumferential coordinates, respectively, G_{xy} is the inplane shear stiffness, and μ_x and μ_y are Poisson's ratios where $\mu_x E_y = \mu_y E_x$. The secant and tangent moduli, E_{sec} and E_{tan}, are evaluated at the buckling strain with the use of an appropriate stress-strain curve. The quantity μ (eq. (14)) is calculated from the elastic value of Poisson's ratio, μ_e, and the elastic modulus, E, of the material involved.

Construction of σ-ϵ curve for equivalent stiffening grid layer.- A stress-strain curve for the equivalent stiffening grid layer of the shell wall can be constructed as indicated by the schematic curve in figure 2. The slope of the linear region of the curve is determined from equation (1). The nonlinear region is constructed from the stress-strain curve of the material involved where the equivalent stress, σ_{eq}, and strain, ϵ_{eq}, are given by the following equations:

$$\left.\begin{aligned} \sigma_{eq} &= g\,\frac{E_{eq}}{E}\,\sigma \\ \epsilon_{eq} &= g\epsilon \end{aligned}\right\} \qquad (15)$$

The factor, g, in these equations is related to the onset of plasticity and depends on the orientation of the stiffening grid system with respect to the loading. For an orientation as shown in figure 1 (assuming the cylinder to be loaded in axial compression) g is unity. It can be shown, however, that when the stiffening grid layout is rotated 90^{o} with respect to the direction of loading, the onset of plastic deformation is delayed and g takes on a value of 3/2. The resulting stress-strain curve constructed by this method can be used in conjunction with equations (4) through (14) to calculate the equivalent orthotropic constants when the grid experiences strains beyond the proportional limit.

Buckled-skin properties.- The equivalent orthotropic constants, equations (4) through (14), can also be used to describe the stiffness contributions of the buckled skin by assuming that the postbuckling response of the triangular skin plate can be treated in the same way as material plasticity. A loading-strain curve was generated for the skin (neglecting the effects of curvature) by performing a nonlinear analysis of a representative triangular plate in uniaxial compression using the STAGS computer code (ref. 10). The bifurcation load from a linear prebuckling stress state was also determined with the STAGS code. In applying the STAGS code for both the bifurcation and nonlinear analyses it was convenient to represent the structure as the rectangular region shown in figure 3, which represents the portion of skin shown in the inset. (Due to structural symmetry the behavior of the model shown should be representative of the structure.) The edges at $y = 0$ and $y = h$ are assumed to have zero normal deflection and constant v-deflection to approximate the restraint of the actual stiffening grid members. The edges at $x = 0$ and $x = \frac{h}{\sqrt{3}}$ have zero slope due to symmetry and are allowed constant u-deflections. Along the diagonal it is assumed that zero normal deflection, $w = 0$, approximates the restraint of a diagonal stiffening grid member. The particular model shown in figure 3 is analyzed for the case of loading in the x-direction and has an 11×11 finite-difference grid. The case for loading in the y-direction was also examined with a model having a 9×15 finite-difference grid. The loading for both cases is applied as a uniform inplane edge displacement ($u = \text{Constant}$ or $v = \text{Constant}$) which approximates a uniform strain field for either N_x or N_y loadings. From the STAGS bifurcation analysis it was found that the buckling stress for an equilateral triangular plate, loaded in uniaxial compression in either the x- or the y-direction, can be calculated by the following equation:

$$\epsilon_{cr} = \frac{\sigma_{cr}}{E} = \frac{6.23}{1 - \mu^2}\left(\frac{t}{h}\right)^2 \qquad (16)$$

In order to perform a STAGS nonlinear analysis of the model shown in figure 3, a small initial imperfection must be assumed to trigger the postbuckling response. For this analysis a shape that approximates the buckling mode was used which is given by the following equation:

$$w_i = 0.00001 \sin\left[\frac{\pi}{h}\left(\sqrt{3}x - y\right)\right] \sin\frac{\pi y}{h} \tag{17}$$

The variation of the average inplane stress resultant, N_x, with respect to strain in the x-direction is shown by the solid curve in figure 4. The abrupt changes in the curve correspond to the onset of buckling and changes in buckle pattern and, since the symmetric boundary conditions at $x = 0$ and $x = \frac{h}{\sqrt{3}}$ exclude antisymmetric buckling modes in the x-direction, the first abrupt change after buckling occurs as the mode pattern changes from one to three half waves and the next occurs at the change from three to five half waves. Additional mode changes could not be detected although they probably would appear if a very fine finite-difference grid were used. Thus, it should be realized that the curve is only approximate in the very high strain range. On the other hand, it is not clear that these mode changes would actually occur at the load levels indicated but may be considerably delayed. Such mode changes have been observed in long rectangular panels (ref. 11) but were not observed in the isogrid cylinder test of reference 4.

The dashed curve in figure 4 represents the variation of inplane stress resultant, N_y, with respect to strain, ϵ_y. As can be seen, the two models behave similarly in the mutual range of loadings investigated. Thus, it is assumed that a single stress-strain curve representing loading in either direction is applicable for estimating the buckled-skin properties. This curve is presented in figure 5 where the stress is nondimensionalized with respect to the bifurcation stress, σ_{cr}, and the strain is nondimensionalized with respect to the strain at the bifurcation load, ϵ_{cr}; thus, this chart may be generally applied to any equilateral triangular plate in uniaxial compression. It should be remembered when using the curve in figure 5 that some accuracy is probably lost at large values of ϵ/ϵ_{cr}; therefore, this portion of the curve is shown as a dashed line.

In order to calculate the equivalent orthotropic constants for the buckled skin using equations (4) through (14), the values of E_{sec} and E_{tan} are required. Figure 6 gives the variations of the respective moduli as a function of strain. The moduli are nondimensionalized with respect to the elastic material modulus, E. As with figure 5, figure 6 is also generally applicable to any equilateral triangular plate in uniaxial compression.

Calculation of Buckling Load

Once the stress-strain curves are determined for the skin and equivalent stiffening grid layer throughout the strain range of interest, the curves can be combined to obtain a

loading-strain curve that represents the behavior of the cylinder wall. The calculation of the buckling load proceeds as follows: a strain is assumed and the corresponding stiffening grid layer properties are determined for this strain from equations (4) through (8) applied to the stiffening grid stress-strain curve. The skin-layer properties are also determined from equations (4) through (8) with the necessary secant and tangent moduli determined from figure 6 and with equation (16) used to evaluate ϵ_{cr}. The layer properties are input to the shell-of-revolution analysis program, and a buckling stress resultant is calculated. This loading will not, in general, agree with the stress resultant from the loading-strain curve of the cylinder wall at the assumed strain; thus, the strain is adjusted appropriately, and the process is repeated. The buckling strain sought, normally, can be easily obtained in no more than three iterations of this process. It is important to realize that the average strain is used in this procedure and variation of strain through the wall thickness due to local wall bending is not taken into account.

APPLICATION OF ANALYSIS PROCEDURE

Test Specimen

The isogrid-cylinder test specimen reported in reference 3 is shown mounted to the lower portion of the loading fixture in the photograph in figure 7. The cylinder had a 3.05-m diameter and was 0.946 m in length. It was assembled from three curved panels that were initially machined from flat plates of 2024-T851 aluminum alloy and then roll-formed to the proper curvature. The fabrication technique is discussed in detail in reference 1. Note the short "transition section" at the top edge of the cylinder characterized by the square pockets. A similar section occurs at the bottom edge. These transition sections were introduced to help distribute the hard-point loading of the longitudinal stiffening grid members into the supporting structure. A steel loading ring, which is part of the supporting structure and to which the lower edge of the cylinder is attached, is also shown in figure 7. The top edge of the cylinder would be attached to a similar loading ring when installation of the cylinder in the test fixture is completed. The loading rings are included as part of the present shell-of-revolution analysis model to reduce effects of unknown boundary conditions.

Construction details of the overall layout of the structure are shown in figure 8 along with detail dimensions. The dimensions shown for the typical grid-member cross section are averaged values from five circumferential stations (station numbers 0, 1, 2, 58, and 59, ref. 4) in the vicinity of peak axial loading. The cylinder was loaded in bending and axial compression so that station 0 is the station at which load peaking was expected and stations 1 and 59 are 6° on either side of station 0 while stations 2 and 58 are 12° on either side of station 0. The loading was applied to the cylinder by two heavy end fixtures actuated by 24 hydraulic jacks as indicated in the photograph in figure 9. The hydraulic

jacks were programed to apply loads that were proportional to their distance from the plane through which the axis of the test specimen passed. The loading fixtures upon which the jack loads acted were an order of magnitude greater in stiffness than the test specimen; thus, it is assumed that plane sections of the cylinder remained plane during loading. The photograph in figure 9 was taken when the test cylinder was under load as indicated by the buckled condition of the skin.

Immediately prior to testing, measurements were taken to obtain an indication of the initial imperfection condition of the specimen. The results are shown in figure 10, where the normal imperfection, w_0, is plotted as a function of circumferential coordinate, θ, in the vicinity of the cylinder midlength.

Analytical Model

The model for the shell-of-revolution analysis is shown in figure 11. It is necessary to consider only half the length of the shell due to structural symmetry; thus, the model is composed of three longitudinal segments: (1) the isogrid cylinder, (2) the transition section, and (3) the steel loading ring. Note that the skin layer is located within the 2.48 cm thick equivalent stiffening grid layer as shown in the inset. A discrete ring with section properties of a typical grid member is attached at the isogrid transition-section interface. The transition section is treated as a single skin layer stiffened by 180 equally spaced, eccentric, longitudinal stiffeners having section properties of a typical grid member. These stiffener properties are averaged in the analysis. The steel loading ring contains 180 equally spaced mild steel bolts, 0.635 cm diameter and 12.6 threads per cm, whose stiffness properties are also averaged in the analysis. In addition, the eccentricity of the bolts is taken into account. The full stiffness of the bolts, based on the elastic modulus of 207 GN/m^2, cannot reasonably be used in the analysis since resulting bolt stresses would be unrealistically high; however, failure of the bolts was not observed during the test since the bolts were very short and loaded in compression. In order to maintain bolt stresses at a reasonable level for mild carbon steel, a reduced modulus is used partially to account for the high plastic strains that must have been present. For prebuckling stress analysis, bolt stiffness is based on 10 percent of the elastic modulus and, for the buckling analysis, bolt stiffness is based on 5 percent of the elastic modulus. Additional calculations made with varying bolt stiffnesses showed results were insensitive over a wide range of stiffness values. Classical simple-support boundary conditions (including u free and $v = 0$) are assumed to apply at the edge of the loading ring. Subsequent calculations were also made for clamped boundary conditions and showed no significant effect on buckling load.

Equivalent Layered-Wall Properties

A compressive stress-strain curve was determined for 2024-T851 aluminum alloy by performing a laboratory test of a sample cut from the test specimen. The results of this test are shown by the dashed curve in figure 12. As indicated in this figure, the slope of the linear portion of the curve was found to be 77.2 GN/m^2, a value that is slightly greater than the accepted value of 73.8 GN/m^2 for 2024 aluminum alloy. Since the test specimen cut from the isogrid cylinder was smaller than standard coupon size, however, and the flatness of the edges could not be carefully controlled, it was decided to adjust the curve to yield the accepted value of Young's modulus by assuming that the measured stress was accurate and any error was in measured strain. It is interesting to note that the stress-strain curves given for 2024-T851 aluminum alloy in reference manuals show much lower stress levels in the plastic range than the adjusted curve. Thus, it is probable that during fabrication, the machining of the stiffening grid from solid plate and the subsequent rolling to proper curvature work-hardened the material to increase its ultimate stress capability.

The equivalent stiffening grid layer behavior under loading is constructed (as discussed in connection with fig. 2) with the aid of the solid curve in figure 12 and equations (1) and (2), where E in equation (1) is replaced by E_{sec} from figure 12. The result is shown by the short-dashed curve in figure 13. The elastic-plastic behavior of the buckled skin in uniaxial compression is determined with the aid of figure 5 and equation (16). This curve is shown by the long-short dashed curve in figure 13. The loading-strain curve for the equivalent two-layer shell wall is determined by adding these two curves and is shown by the solid curve in figure 13.

Nonlinear Effects on Inplane Loading

The maximum inplane stress resultant, N_x, for a cylinder loaded in bending due to moment M and axial compression due to axial load, P, can be calculated with the classical formula:

$$N_x = \frac{P}{2\pi R} + \frac{M}{\pi R^2} \tag{18}$$

The deviation of inplane loading from this classical value when nonlinear effects occur is investigated using the assumption that the strain remains linear through a cross section of the cylinder (plane sections remain plane) during loading. The results of this calculation are shown in figure 14 for the ratio $\frac{M}{PR} = 0.5$ (the value maintained during the buckling test of the cylinder). As indicated in the inset, P acts through the center of the cylinder cross section. For a given P and M the actual N_x can be determined from the solid curve in figure 14.

Prebuckling Strains

Prebuckling strains (strains prior to general shell buckling) were calculated with the SRA program using secant stiffnesses for each layer determined with the aid of figure 13. An indication of the accuracy of the computed load-strain curve (fig. 13) is given in figure 15 where the strain measured on the web of the longitudinal stiffener at the location at which maximum inplane loading was expected is compared with theory. Since at this location the strain approaches the average over the wall cross section, the comparison indicates that the constructed load-strain curve adequately represents the behavior of the cylinder.

The meridional variation of extreme fiber strain at the inner flange of a longitudinal stiffener is shown for two load levels in figure 16. At 47 percent of buckling there is good agreement, although some evidence of wall bending, due to initial imperfections not accounted for in the axisymmetric analysis, is exhibited by the data. At 98 percent of the buckling load the strain data clearly indicate that buckling is imminent. The axisymmetric stress analysis cannot be expected to predict the antisymmetric character of the data. The strain data oscillate about the theoretical curve, however, indicating general agreement if the bending strains due to buckling are ignored.

Buckling

Structurally perfect model.- In order to determine the buckling load it is necessary to know the strain at the load of incipient buckling so that the proper material properties are used. The iteration procedure used is discussed in the present report in the previous section entitled "Calculation of Buckling Load." Buckling is investigated for two different loading cases: (1) axial compression, and (2) the actual loading, applied on the test specimen, of combined compression and bending. Since the material properties must remain axisymmetric, the latter analysis was made assuming properties occurring at the extreme compression fiber. The method for determining the buckling load for the nonlinear region of the loading-strain curve is shown graphically in figure 17. The dashed curve is the combined loading-strain curve (see fig. 13) for the isogrid cylinder. Buckling results as a function of strain are shown by the solid curves. The intersections of these curves with the dashed curve indicate that the calculated buckling stress resultant and the stress resultant from the loading-strain curve are identical; thus, the iteration process has converged. Note that the predicted buckling load for the case of axial loading is essentially the same as that predicted for the case of bending plus axial loading.

The short-long dashed curve labeled "Orthotropic cylinder buckling equation" was obtained from equations presented in reference 12 in which an exact solution is derived for buckling of an orthotropic cylinder with an arbitrary location-of-reference surface. Full bending-extension coupling and shear-twist coupling are included. Boundary conditions

are classical simple supports. For this analysis the boundary conditions were applied at the interface of the steel loading ring with the transition section. The orthotropic stiffnesses were calculated as a function of strain exactly as for the shell-of-revolution analysis. The prediction is about 5 percent below the results from the shell-of-revolution analysis; the difference is probably due to unrealistic boundary conditions used in the simple analysis as well as omission of such details as the discrete rings and the increased stiffnesses of the transition sections. It is true, however, that for simply supported, isogrid cylinders the orthotropic-cylinder buckling equation can yield accurate results for strains above the proportional limit when used in conjunction with the procedure presented herein.

The buckling mode shapes for the actual loading of combined bending and axial compression applied to the test specimen, considering both symmetric and antisymmetric meridional buckle mode patterns, are shown in figures 18 and 19, respectively. The calculated buckling load was found to be critical for the symmetric mode; however, the antisymmetric mode was also investigated since the experimental strains shown in figure 16(b) indicate a tendency for the shell to buckle into an antisymmetric meridional wave. The calculated buckling load for the antisymmetric mode was found to be only 1 percent greater than that for the symmetric mode.

Effects of initial imperfections.- The effects of initial imperfections on buckling load for the model under uniform axial loading are also investigated with the SRA computer code. The imperfection-sensitivity analytical formulation is based on the method of reference 13 and is presented in detail in reference 14. The cylinder is assumed to have an axisymmetric imperfection of parabolic shape (negative Gaussian curvature) with maximum amplitude occurring at the midlength of the cylinder and equal to the average of the measured imperfections given in figure 10 (0.15 cm). The buckling loads for various values of the circumferential wave number, n, $(0 \leq n \leq 9)$ as a function of Δw_o, where Δw_o is the peak deviation of initial imperfection amplitude from the average value, are then examined. In this study, the nonaxisymmetric component of the imperfection shape is assumed to have the same shape as the buckling mode. The buckle modes where $5 \leq n \leq 9$ are found to be insensitive to initial imperfections. For $1 \leq n \leq 4$, however, imperfection sensitivity is evident, as shown in figure 20. Since the shell was fabricated from three segments, imperfections in harmonics divisible by three could be expected to be most dominant, and it is obvious from figure 10 that, of such harmonics, $n = 9$ is likely to be the most dominant. As stated earlier, however, $n = 9$ is not an imperfection-sensitive mode. There are not sufficient data to make a harmonic analysis of the shape shown in figure 10 but, if it can be assumed that the $n = 3$, 6, and 9 components have equal amplitudes, then the imperfection-sensitive $n = 3$ component would have an amplitude equal to 1/3 of the maximum deviation from the mean. Using this value of

imperfection, a reduction in buckling load of 0.95 could be expected from the imperfections of figure 10.

A similar analysis was performed for a model whose equivalent stiffening grid layer was assumed to remain elastic throughout the loading range. The buckling load of this model corresponded to an $n = 7$ mode shape and only the eigenvalues corresponding to $n \geq 5$ were found to be sensitive to initial imperfections, with the reductions more severe than those shown in figure 20. These results suggest that initial imperfection sensitivity of the buckling load is reduced when plastic deformations are involved.

An alternate method for accounting for initial imperfections is available in the NASA space vehicle design criteria for structures (ref. 15) and uses an empirical "knockdown" factor. For a cylinder with proportions of the model analyzed herein, a knockdown factor of approximately 0.65 can be calculated with the equations presented in reference 15, or it may be assumed that the 0.75 knockdown factor, which is recommended in reference 15 for cylinders with closely spaced, moderately large stiffeners, applies. In either case the knockdown is much more severe than that predicted from the imperfection-sensitivity analysis, although it should be noted that the recommendations of reference 15 are based on lower limits of a number of different tests and should be conservative.

Comparison of buckling loads.- The analytical buckling loads are compared with experiment in the following table in which the theoretical values have been adjusted by the factor 0.95 to account for initial imperfections:

Analysis	Applied load	Buckling load, N_x, MN/m	$N_x/N_{x,exp}$
Orthotropic-cylinder buckling equation	Uniform axial compression	0.264	0.97
Shell of revolution	Uniform axial compression	0.279 (m = 0)	1.03
	Bending + Uniform axial compression	0.281	1.04
Experiment	Bending + Uniform axial compression	0.271	1.00

As can be seen, the experimental buckling load is predicted quite accurately by the simple analysis as well as by the shell-of-revolution analysis for either of the two loading cases. A reasonable buckle mode shape can be predicted, however, only by the actual loading case which includes bending.

CONCLUDING REMARKS

An engineering procedure is presented for calculating the compressive buckling strength of isogrid cylinders loaded beyond the material proportional limit and/or the local buckling load of the skin. The procedure is based on the following steps:

(1) The isogrid cylinder is modeled as a two-layer axisymmetric shell, one layer representing the skin and the other representing the stiffening grid system. A third "fictitious layer" of zero stiffeners is introduced to provide separation between the two layers and thereby to maintain proper wall-stiffness properties.

(2) The stiffness of the stiffening grid system is averaged to yield an equivalent "stiffening grid layer" isotropic sheet.

(3) A load-strain curve is constructed for the stiffening grid layer loaded beyond the proportional limit from the stress-strain curve for the material and simple isogrid handbook formulas.

(4) Stiffnesses are determined for the stiffening grid layer in the plastic range from simple formulas based on deformation plasticity theory applied to the constructed stress-strain curve of step (3).

(5) Stiffnesses of the buckled skin are determined from a calculated nonlinear stress-strain curve derived herein and the same plasticity theory used in step (4).

(6) Shell-wall stiffnesses calculated from the above steps are used in existing shell-buckling computer codes or closed-form solutions.

A nondimensional chart is presented which gives the secant and tangent moduli for the buckled skin. This chart has general applicability and is all that is required over simple formulas and standard material-property handbook references for calculating shell-wall stiffnesses.

Comparison of results from the procedure presented herein with experiment shows that:

(1) The theoretically determined axial wall stiffness agrees well with experiment.

(2) The buckling-load prediction (using a shell-of-revolution code in the analysis and accounting for initial imperfections) is about 4 percent greater than experiment.

(3) Theoretical analysis of the effect of imperfections on shell buckling shows the effect to be diminished by plasticity. The excellent agreement with experiment tends to confirm this result since a difference as great as 25 to 35 percent could be expected based on previous test data if the shell was elastic.

Langley Research Center
National Aeronautics and Space Administration
Hampton, Va. 23665
May 18, 1976

REFERENCES

1. Slysh, P.; Ringwald, R. S.; Dyer, J. E.; and Browning, D. L.: Isogrid Weight Optimum Structures. SAWE Paper No. 1063, May 1975.

2. Isogrid Design Handbook. MDC G4295A (Contract NAS 8-28619), McDonnell Douglas Astronautics Co., Feb. 1973. (Available as NASA CR-124075.)

3. Slysh, P.; Dyer, J. E.; Furman, J. H.; and Key, J. E.: Isogrid Structures. AIAA Paper No. 75-816, May 1975.

4. Slysh, P.; and Dyer, J. E.: Conical Isogrid Adapter Structural Test Results. Appendix C – Cylindrical Isogrid Structures. Rep. No. PD 73-0123 (Contract NAS 8-29859), Convair Div., General Dynamics, July 1974. (Available as NASA CR-120463.)

5. Cohen, Gerald A.: Computer Analysis of Ring-Stiffened Shells of Revolution. NASA CR-2085, 1973.

6. Cohen, Gerald A.: User Document for Computer Programs for Ring-Stiffened Shells of Revolution. NASA CR-2086, 1973.

7. Bushnell, David: Stress, Stability, and Vibration of Complex Branched Shells of Revolution: Analysis and User's Manual for BØSØR4. NASA CR-2116, 1972.

8. Svalbonas, V.; and Ogilvie, P.: Numerical Analysis of Stiffened Shells of Revolution – Volume VI of VII. NASA CR-2273, Vol. VI, 1973.

9. Peterson, James P.: Plastic Buckling of Plates and Shells Under Biaxial Loading. NASA TN D-4706, 1968.

10. Almroth, B. O.; Borgan, F. A.; Meller, E.; and Petersen, H. T.: User's Manual for STAGS. LMSC-D358197, Lockheed Missiles & Space Co., Jan. 1974.

11. Stein, Manuel: Loads and Deformations of Buckled Rectangular Plates. NASA TR R-40, 1959.

12. Jones, Robert M.: Buckling of Circular Cylindrical Shells With Multiple Orthotropic Layers and Eccentric Stiffeners. AIAA J., vol. 6, no. 12, Dec. 1968, pp. 2301-2305.

13. Koiter, Warner Tjardus: On the Stability of Elastic Equilibrium. NASA TT F-10833, 1967.

14. Cohen, Gerald A.: Computer Program for Analysis of Imperfection Sensitivity of Ring-Stiffened Shells of Revolution. NASA CR-1801, 1971.

15. Buckling of Thin-Walled Circular Cylinders. NASA SP-8007, 1965. (Revised 1968.)

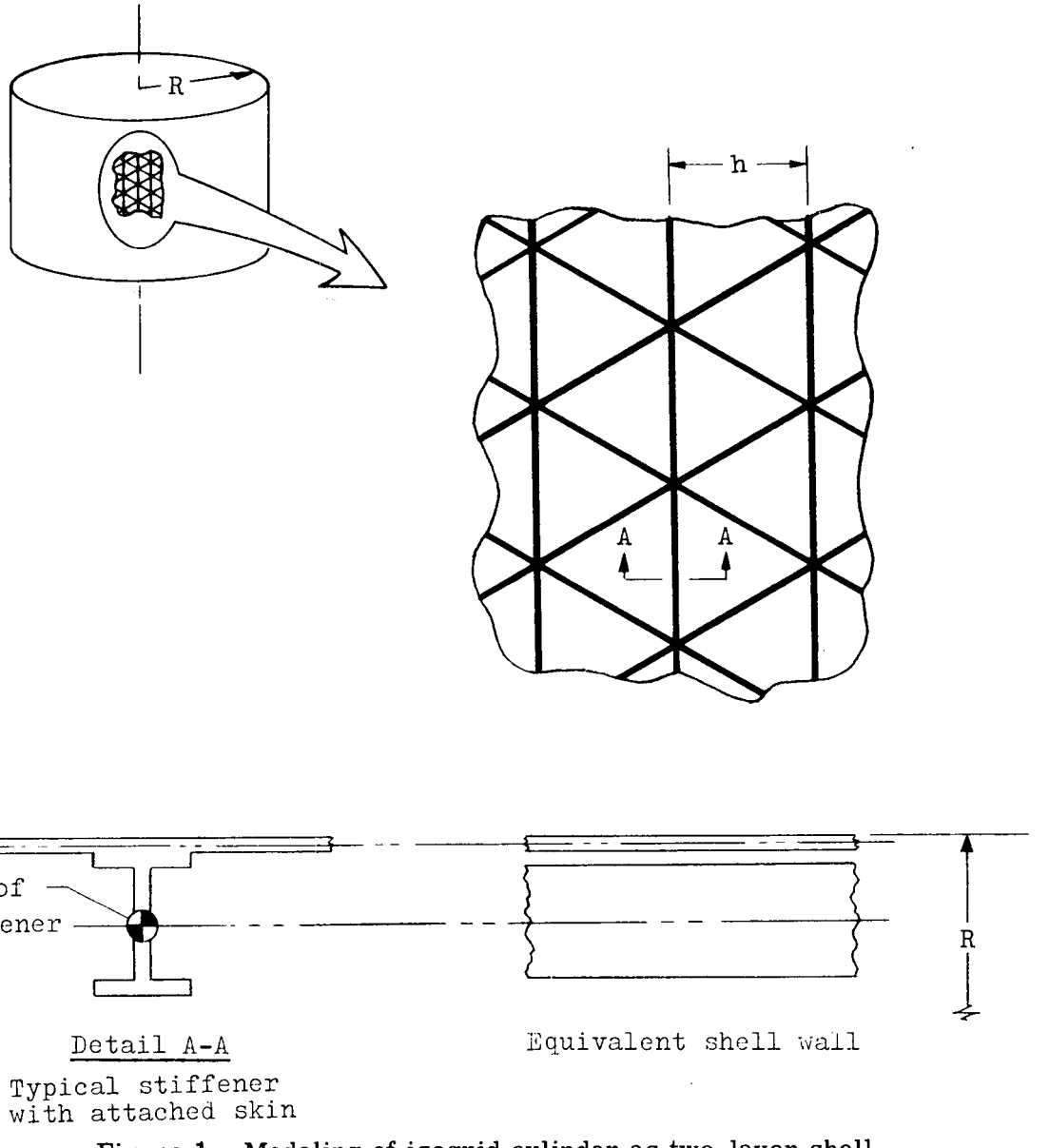

Figure 1.- Modeling of isogrid cylinder as two-layer shell for shell-of-revolution analysis.

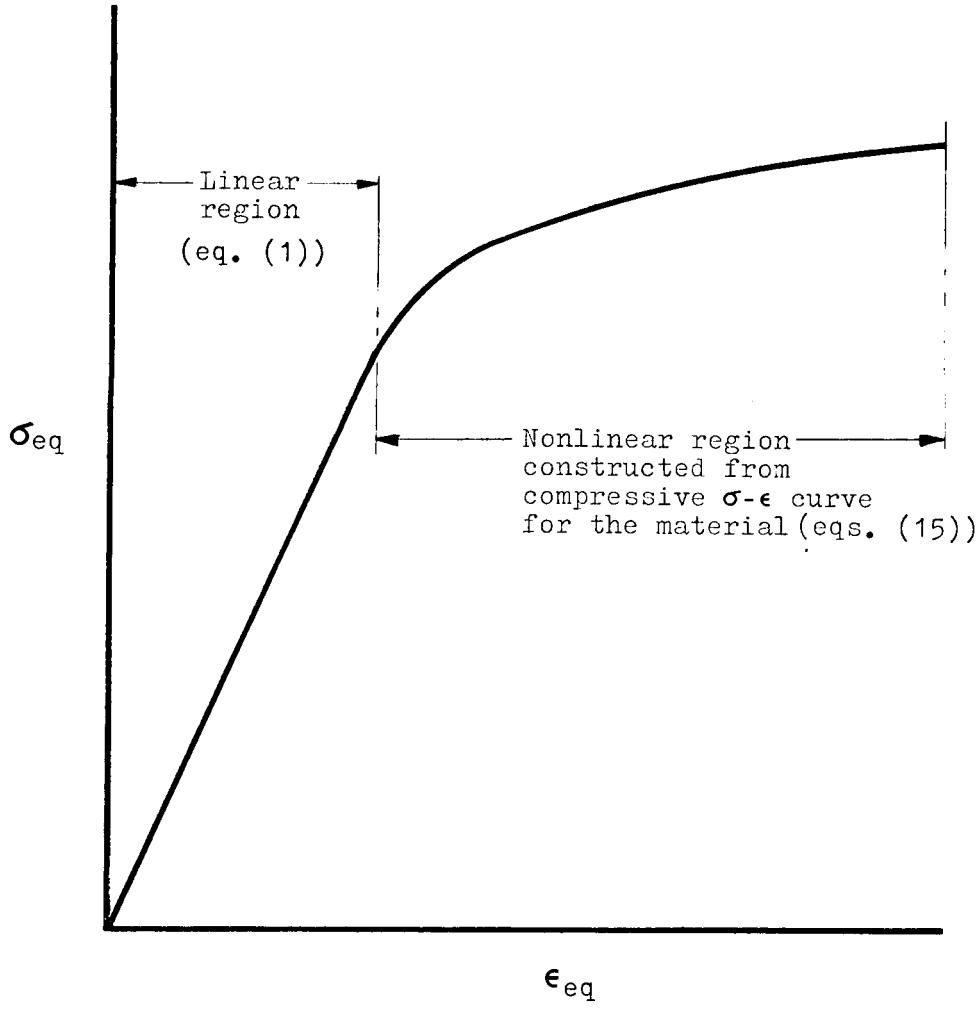

Figure 2.- Schematic of typical stress-strain curve for estimation of equivalent stiffening grid layer properties.

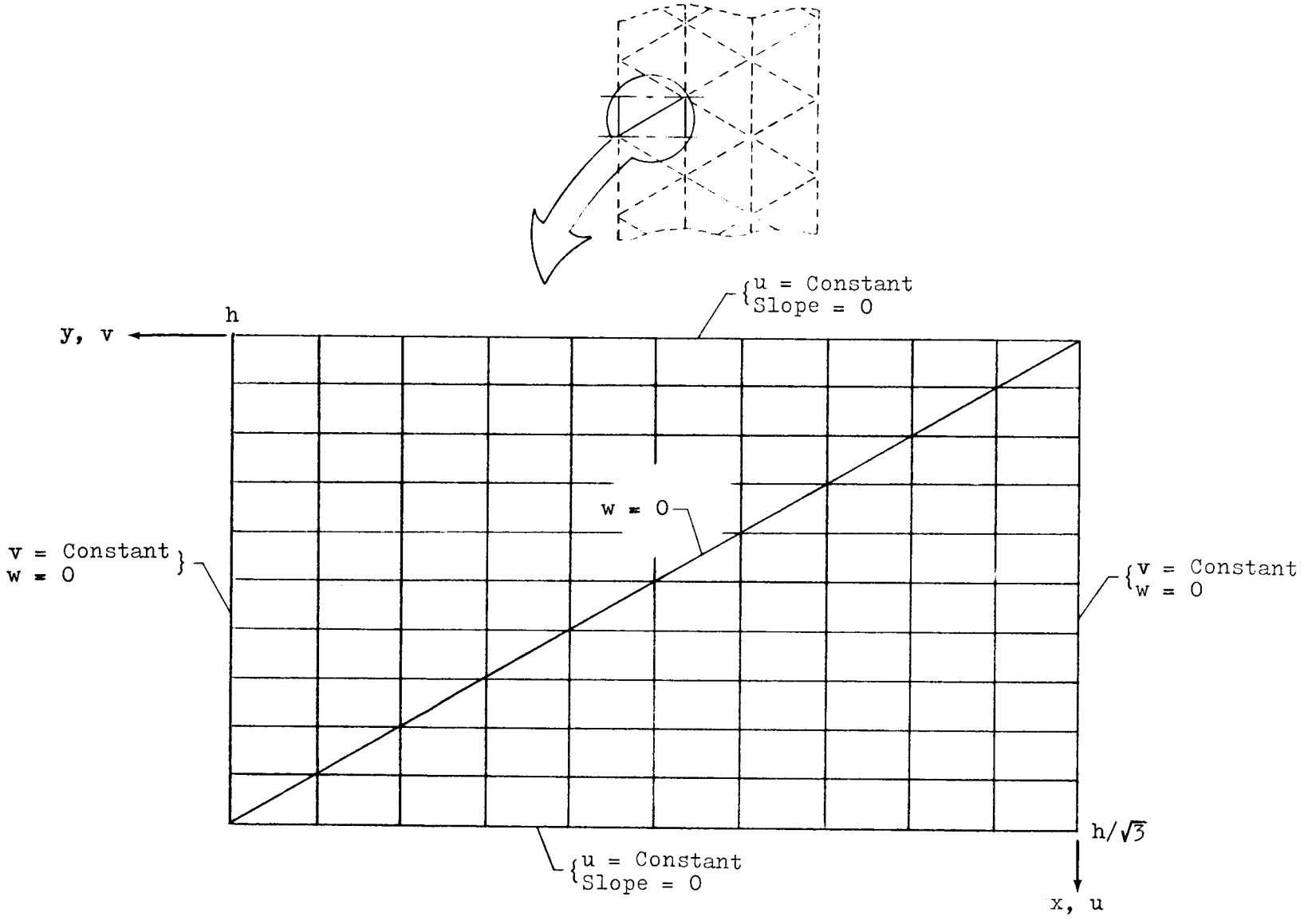

Figure 3.- Representative element of skin of isogrid cylinder wall showing 11 × 11 grid system for STAGS analysis.

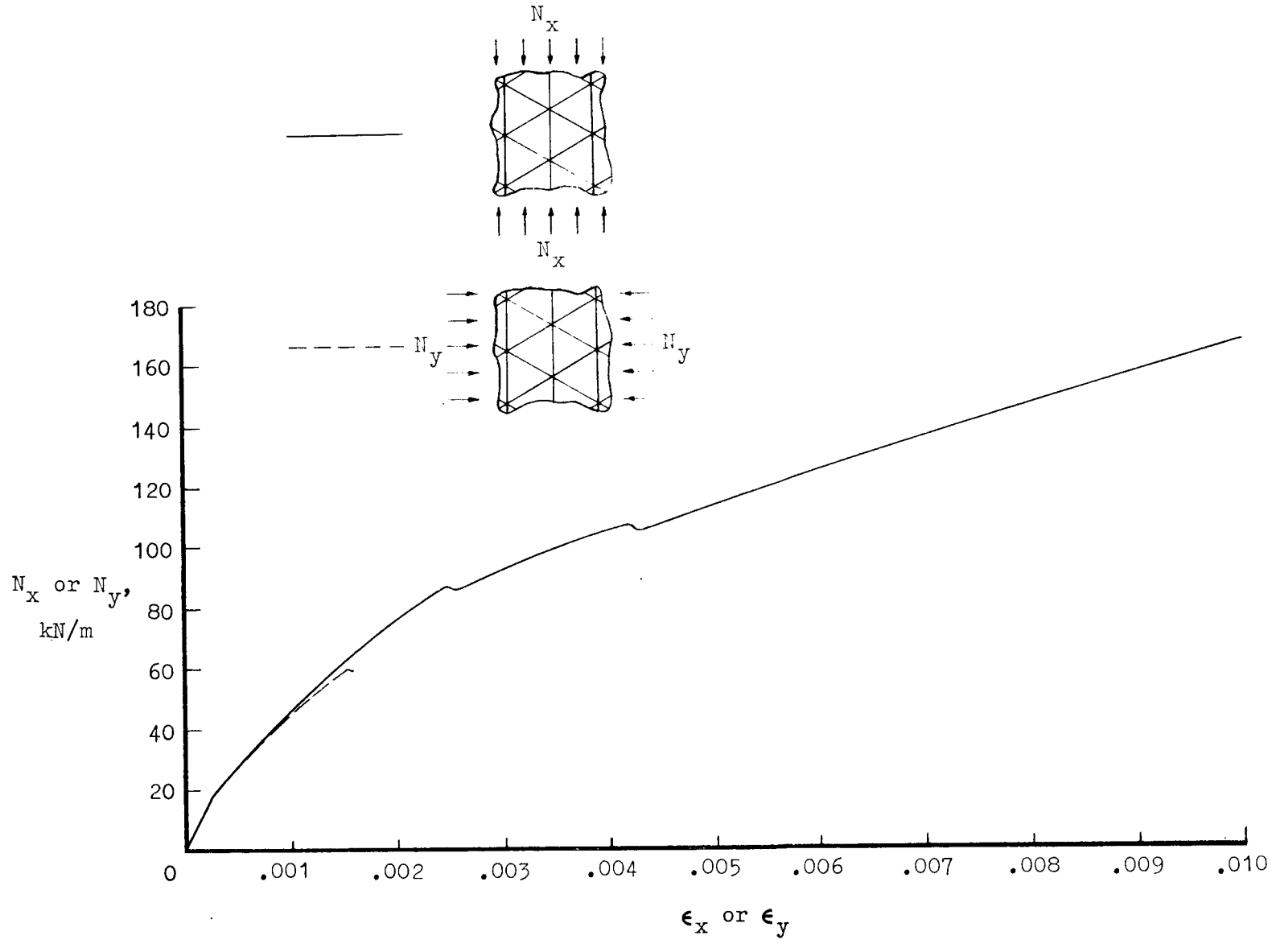

Figure 4.- Variation of inplane stress resultant with uniform strain for skin of isogrid cylinder.

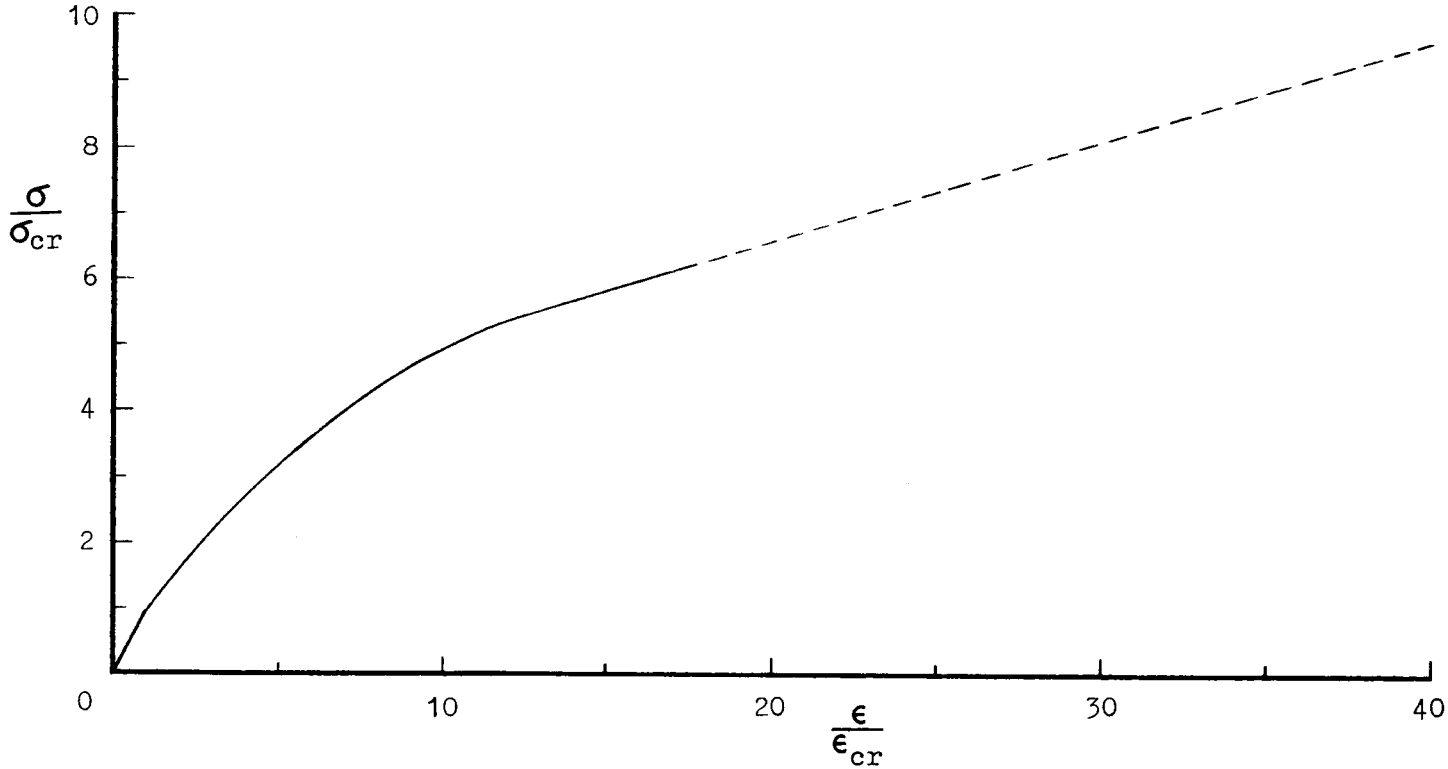

Figure 5.- Stress-strain curve for estimating buckled-skin properties.
(Dashed portion of curve represents an approximation.)

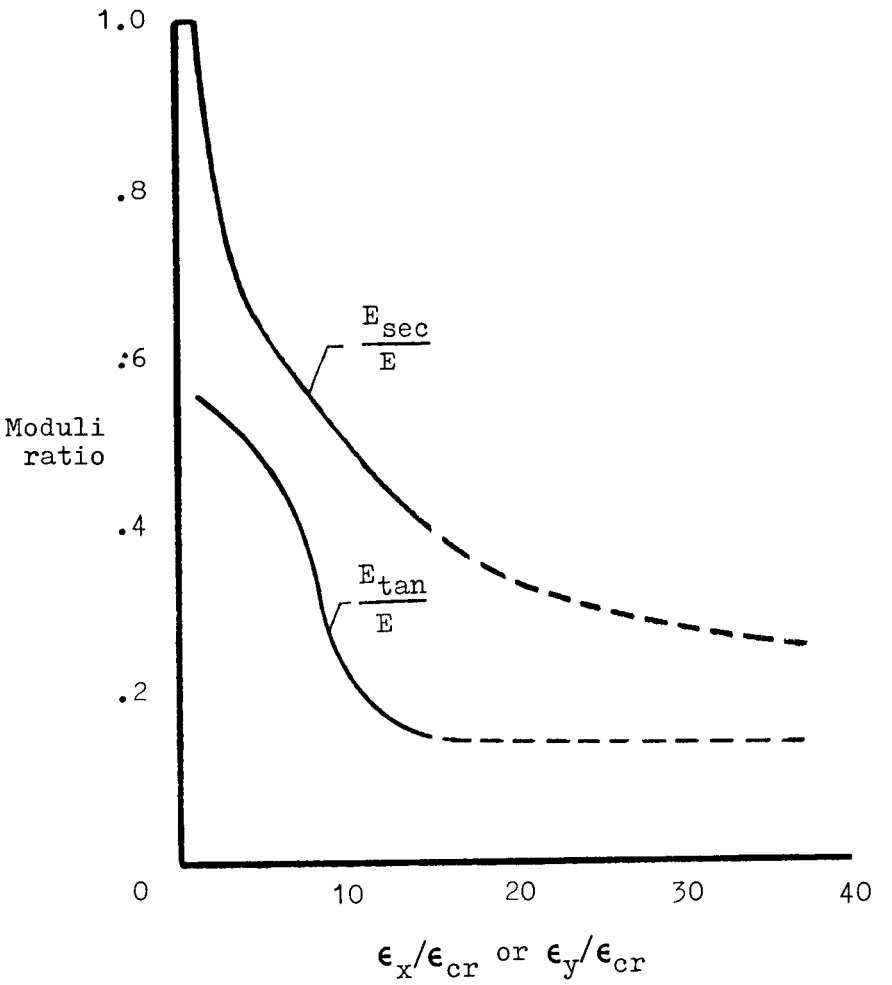

Figure 6.- Variations of secant and tangent moduli with uniaxial strain for skin of isogrid cylinder. (Dashed portions of curves represent approximations.)

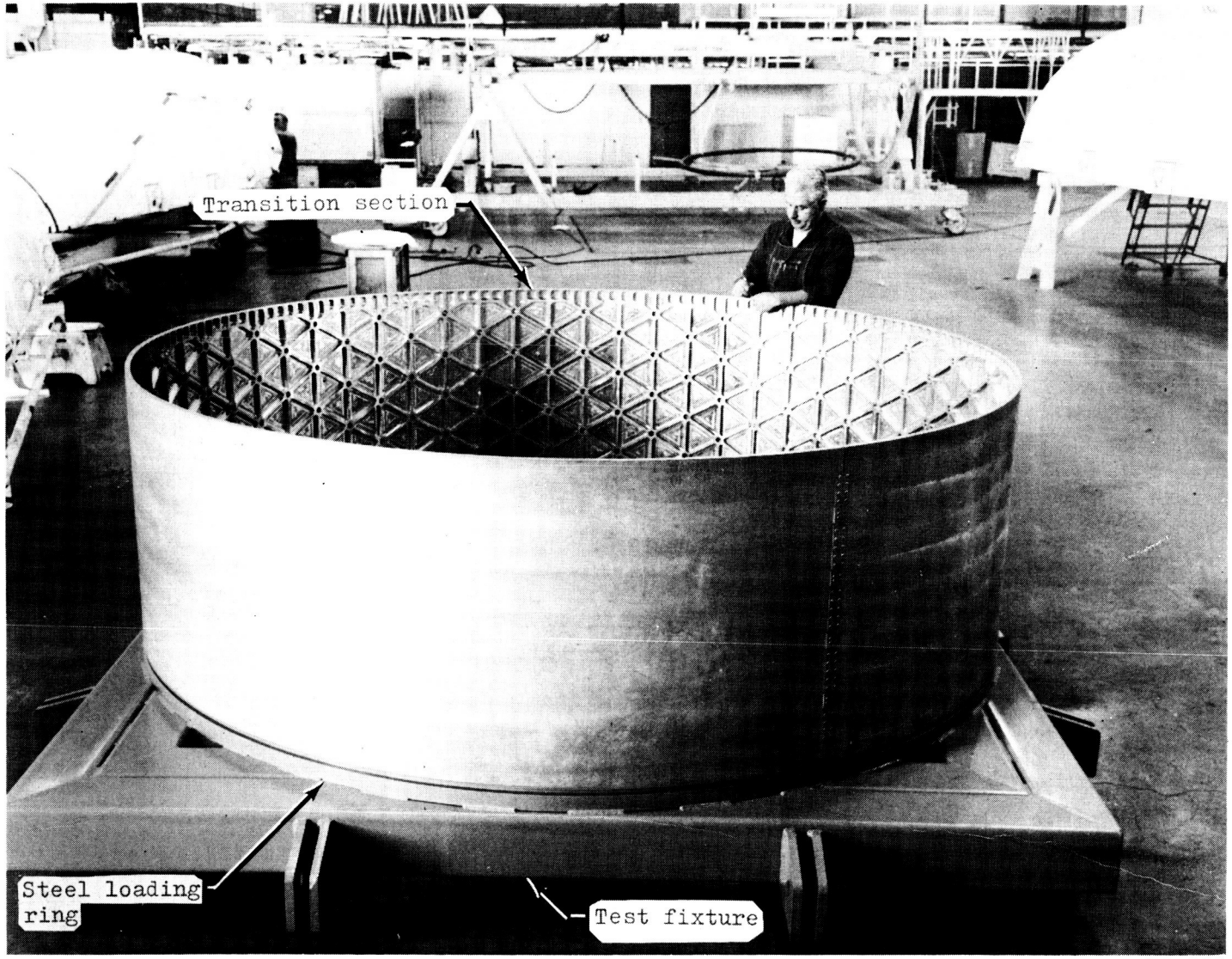

L-76-209

Figure 7.- Test specimen mounted on lower loading fixture.

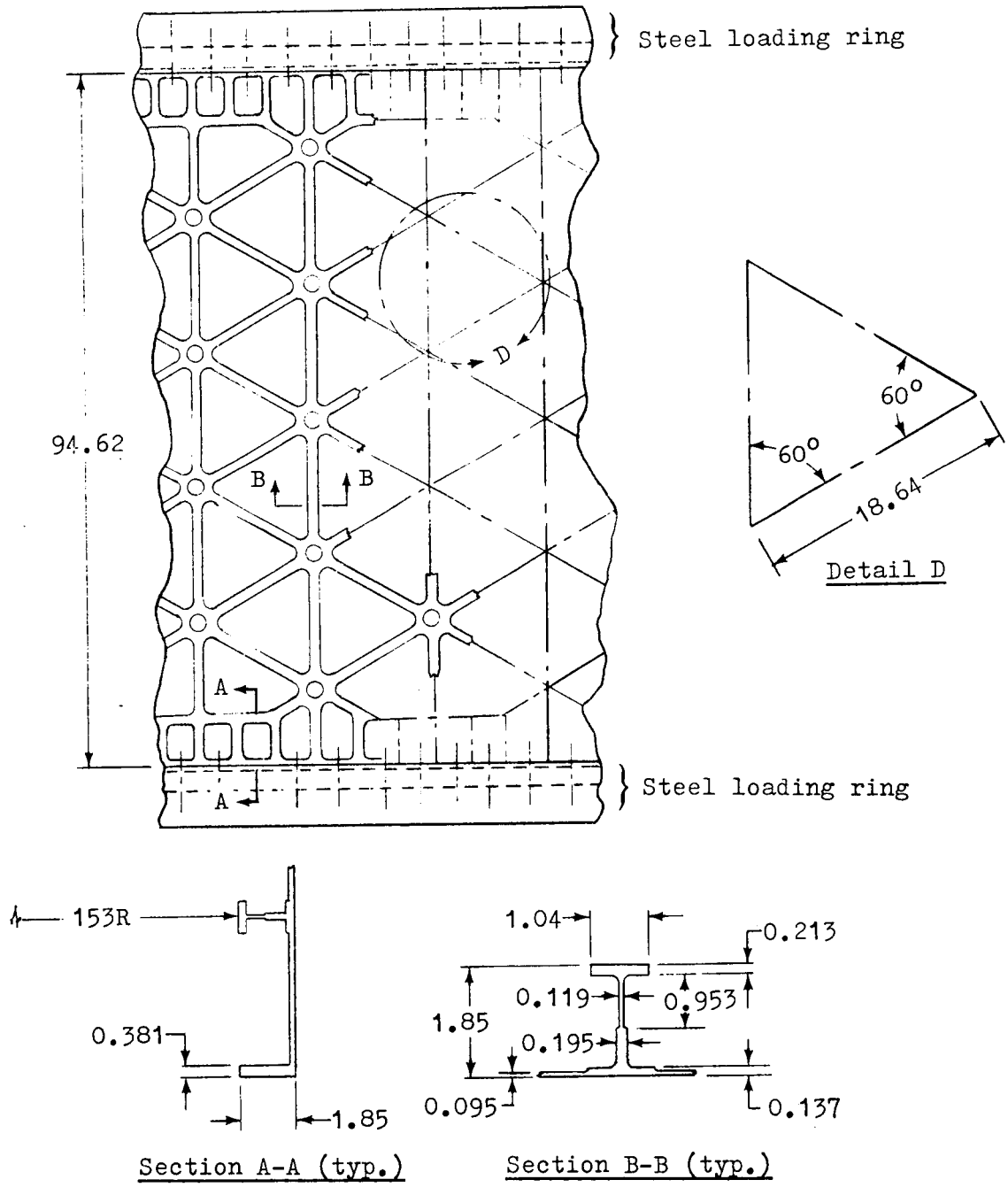

Figure 8.- Construction details of isogrid cylinder (2024-T851 aluminum alloy). (Dimensions in cm.)

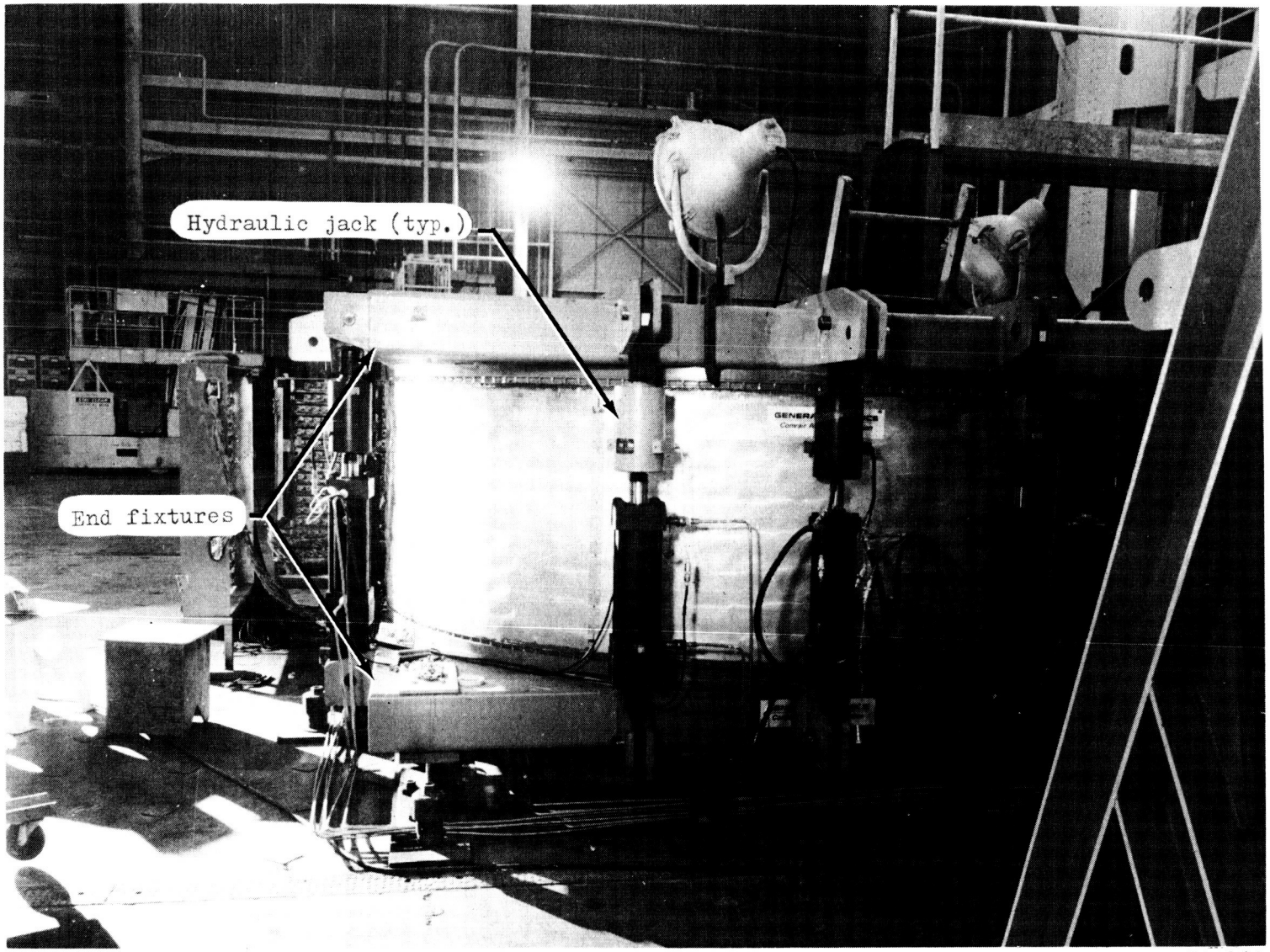

L-76-210

Figure 9.- Test specimen under load showing buckled skin.

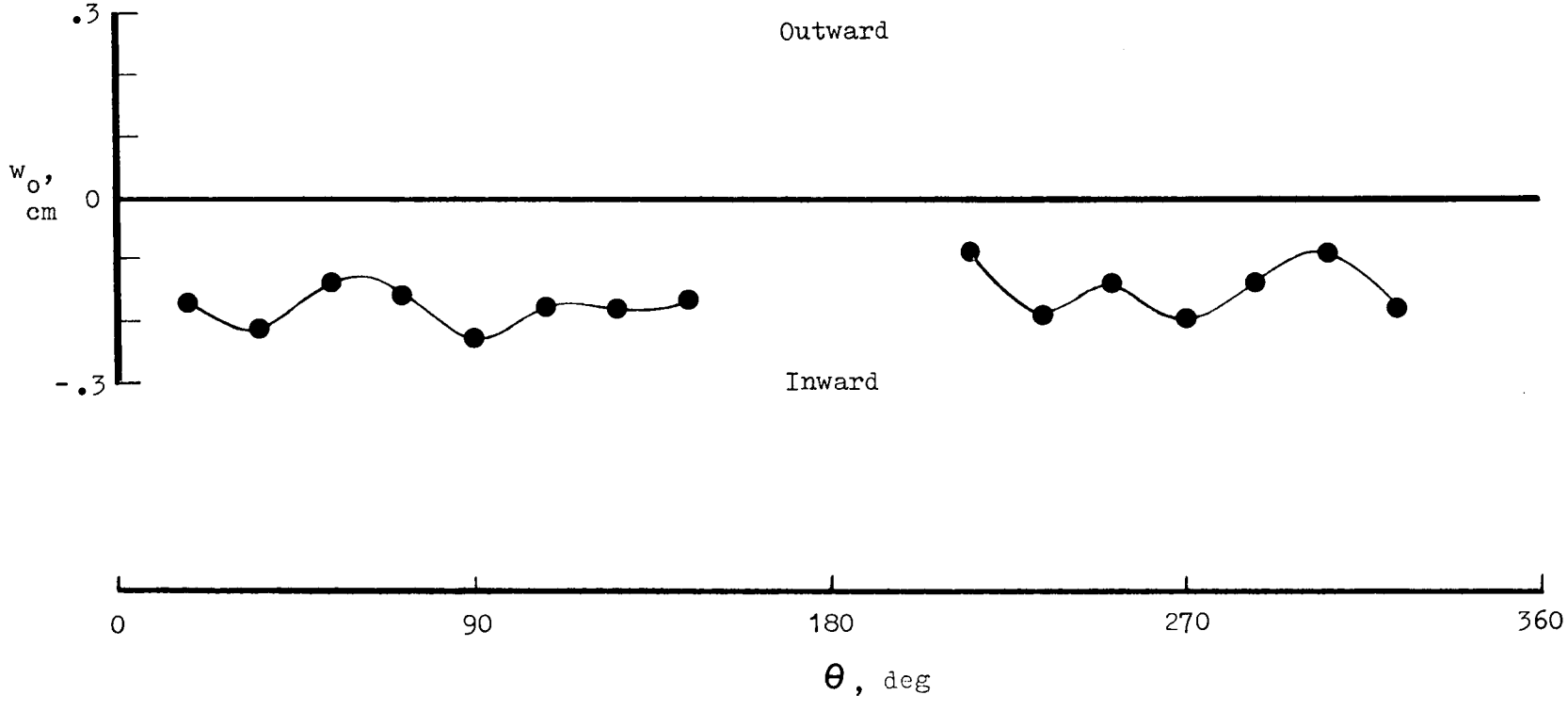

Figure 10.- Measured initial imperfections in vicinity of isogrid-cylinder midlength.

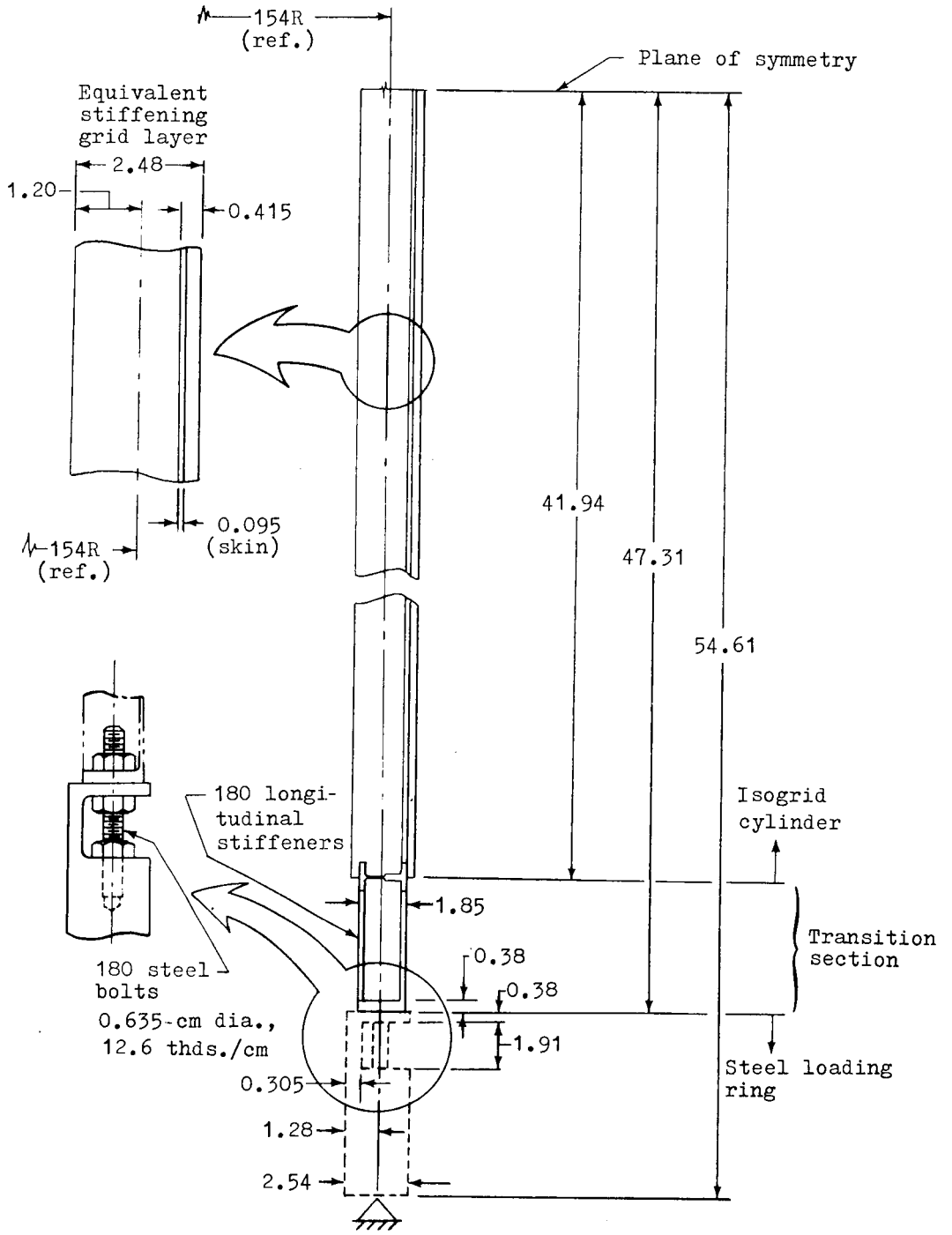

Figure 11.- Model for shell-of-revolution analysis. (Dimensions in cm.)

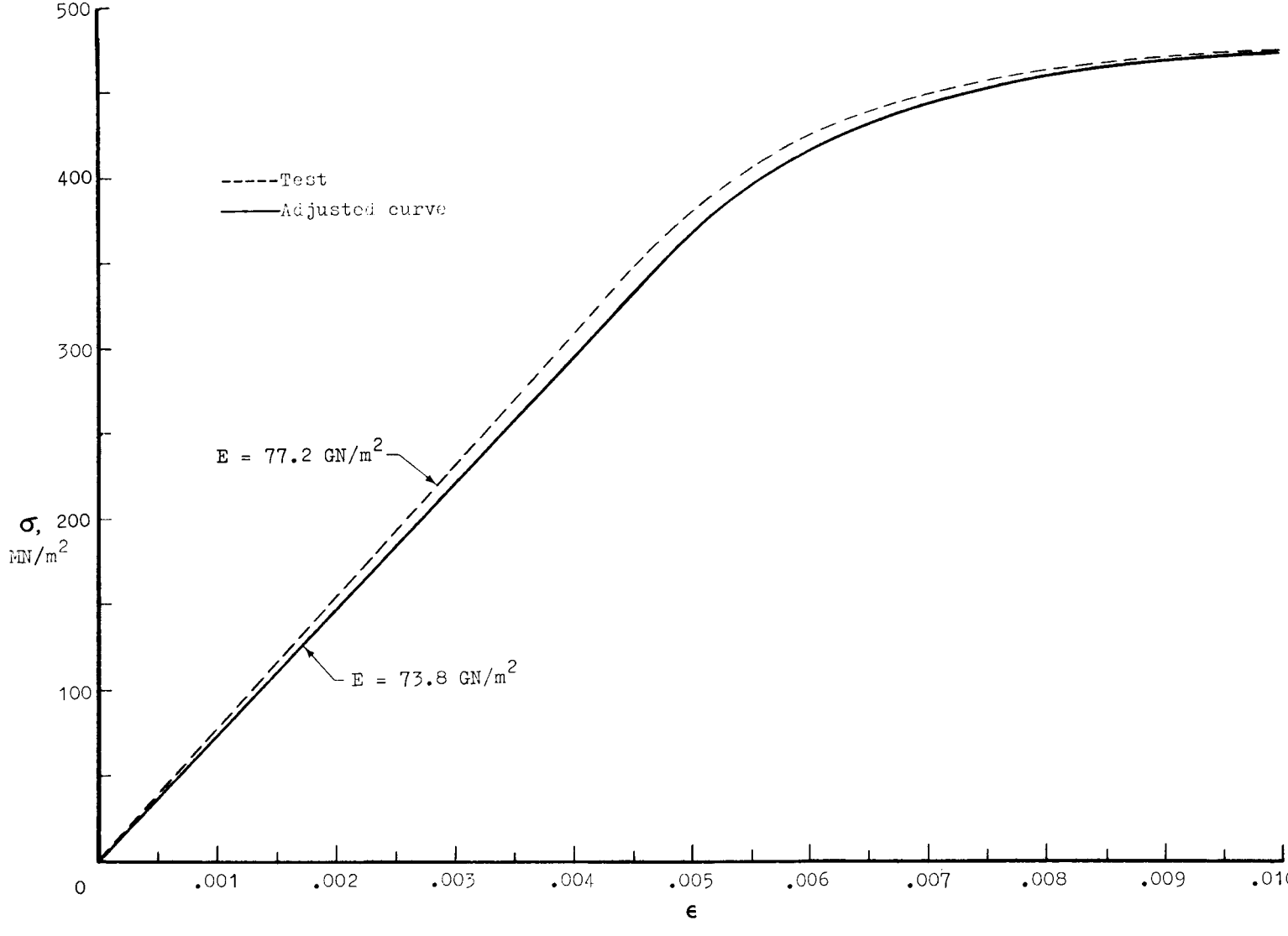

Figure 12.- Compressive stress-strain curve for stiffening grid material, 2024-T851 aluminum alloy.

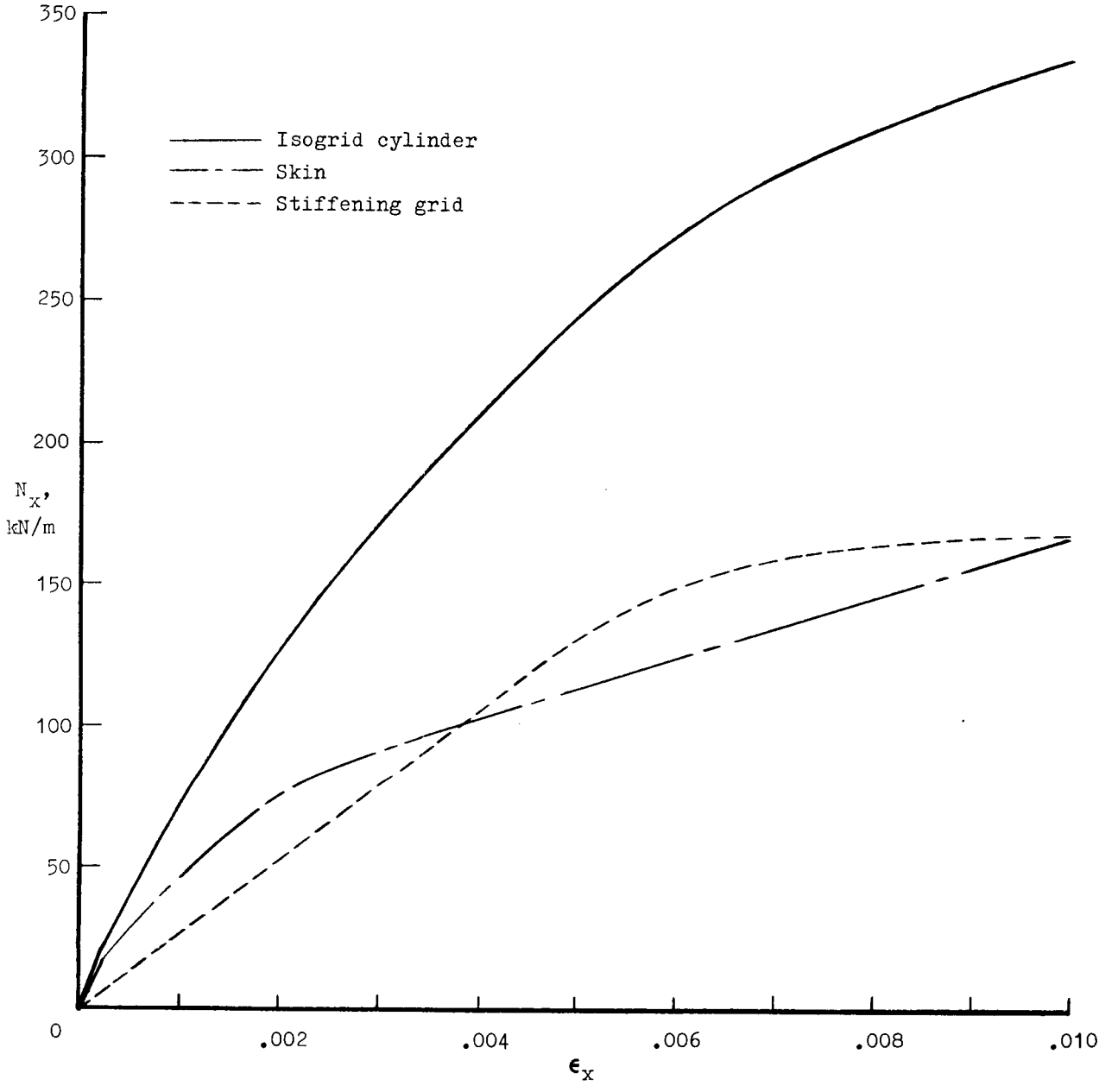

Figure 13.- Constructed loading-strain curve for isogrid cylinder.

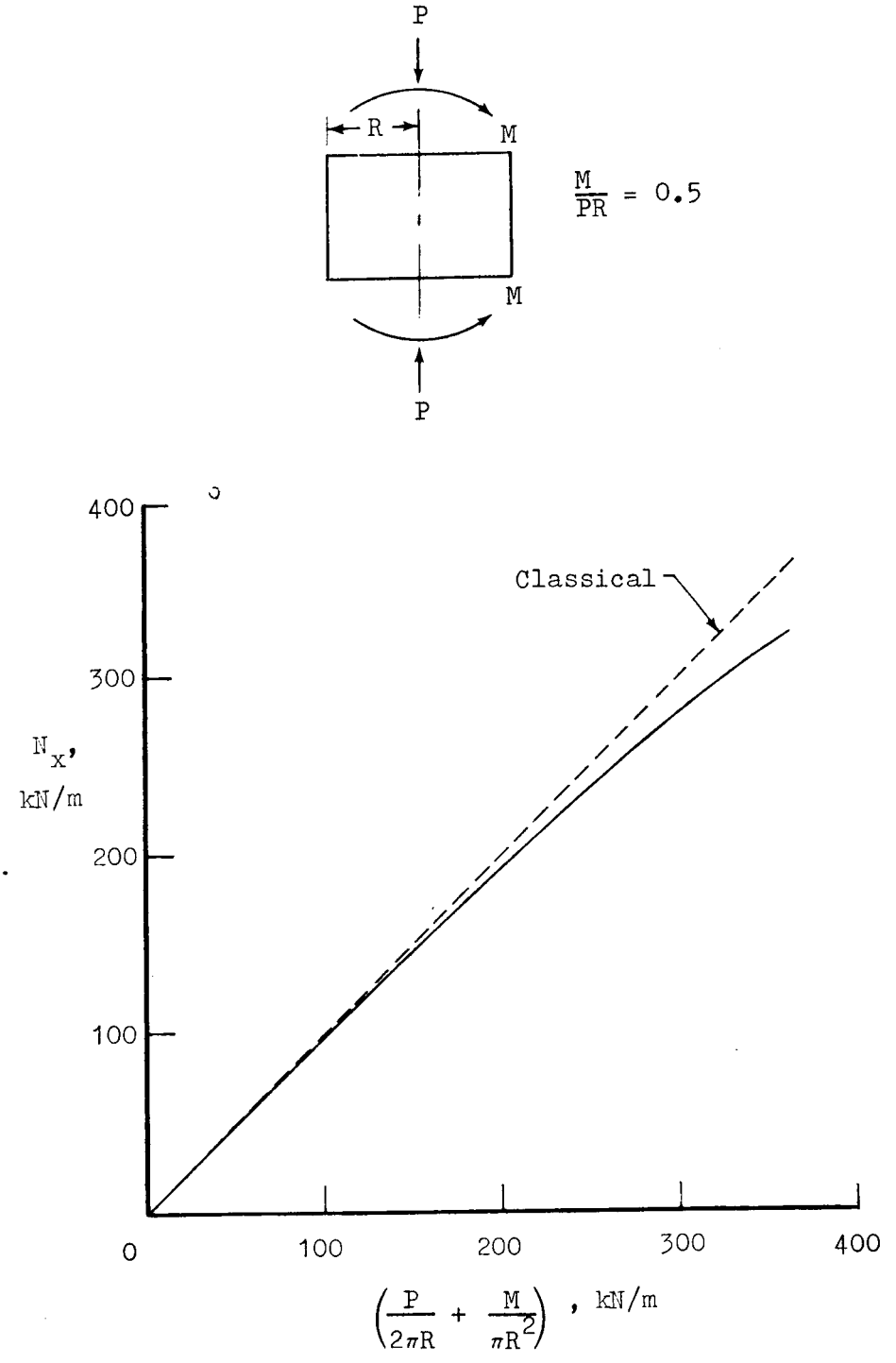

Figure 14.- Deviation of inplane loading from classical value as a result of nonlinear effects.

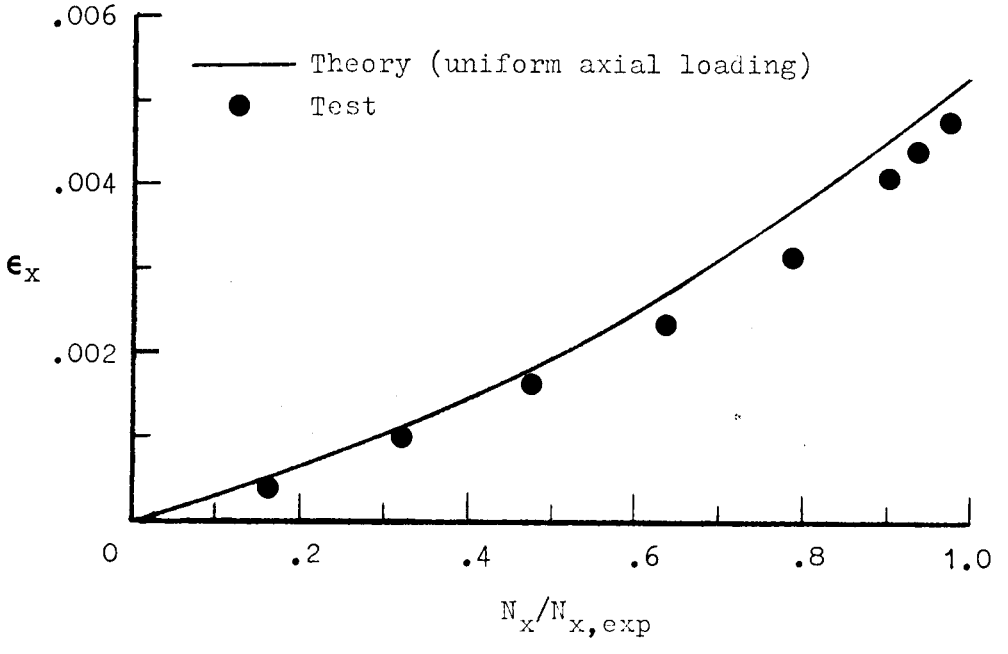

Figure 15.- Comparison of theory and experiment for variation of axial strain in stiffener web with inplane loading. (Gage No. 1166, see fig. 16.)

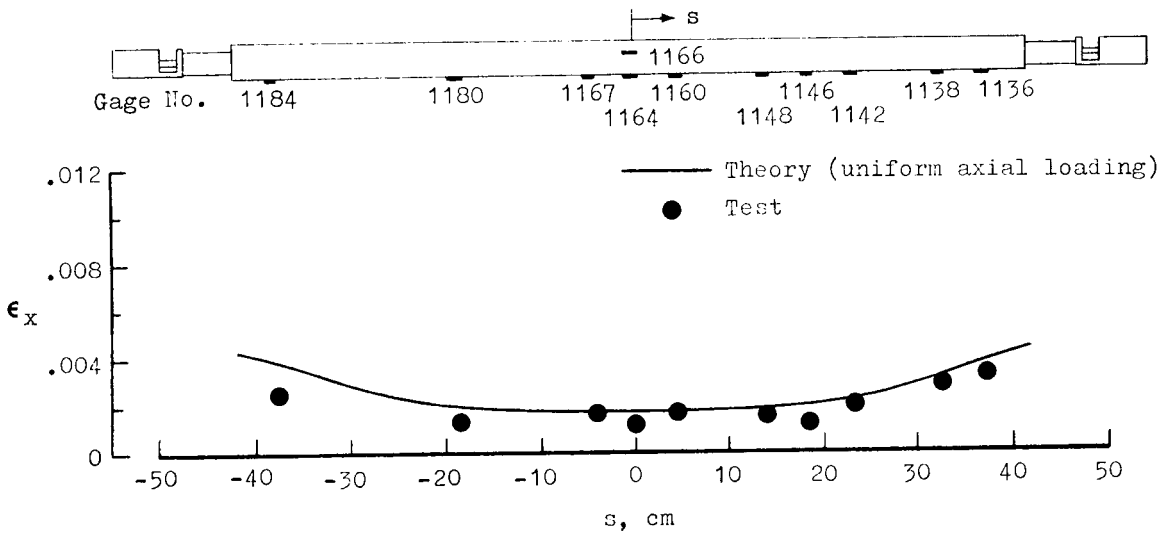

(a) $\frac{N_x}{N_{x,exp}} = 0.47.$

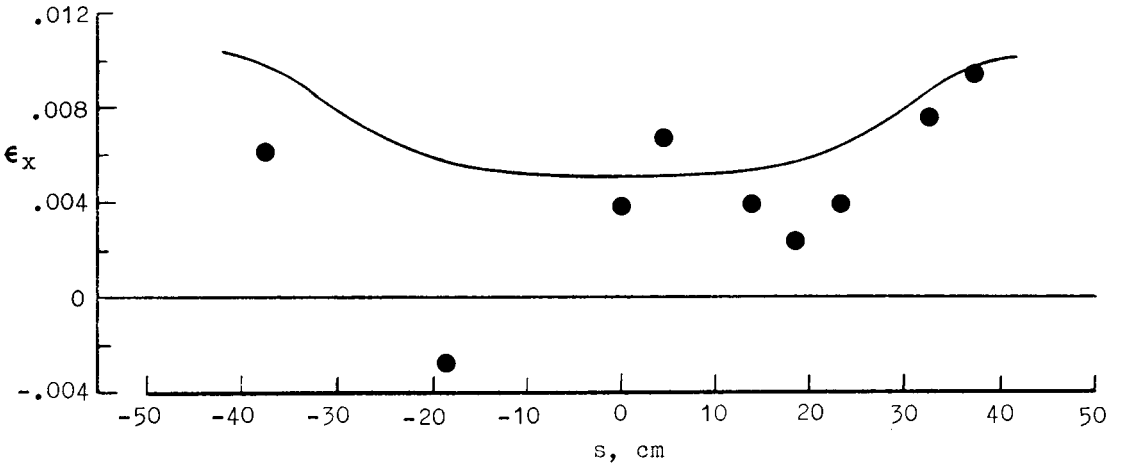

(b) $\frac{N_x}{N_{x,exp}} = 0.98.$

Figure 16.- Comparison with test data of meridional variation of axial strain of extreme fiber of inner flange of longitudinal stiffener. (Gage notation from ref. 4.)

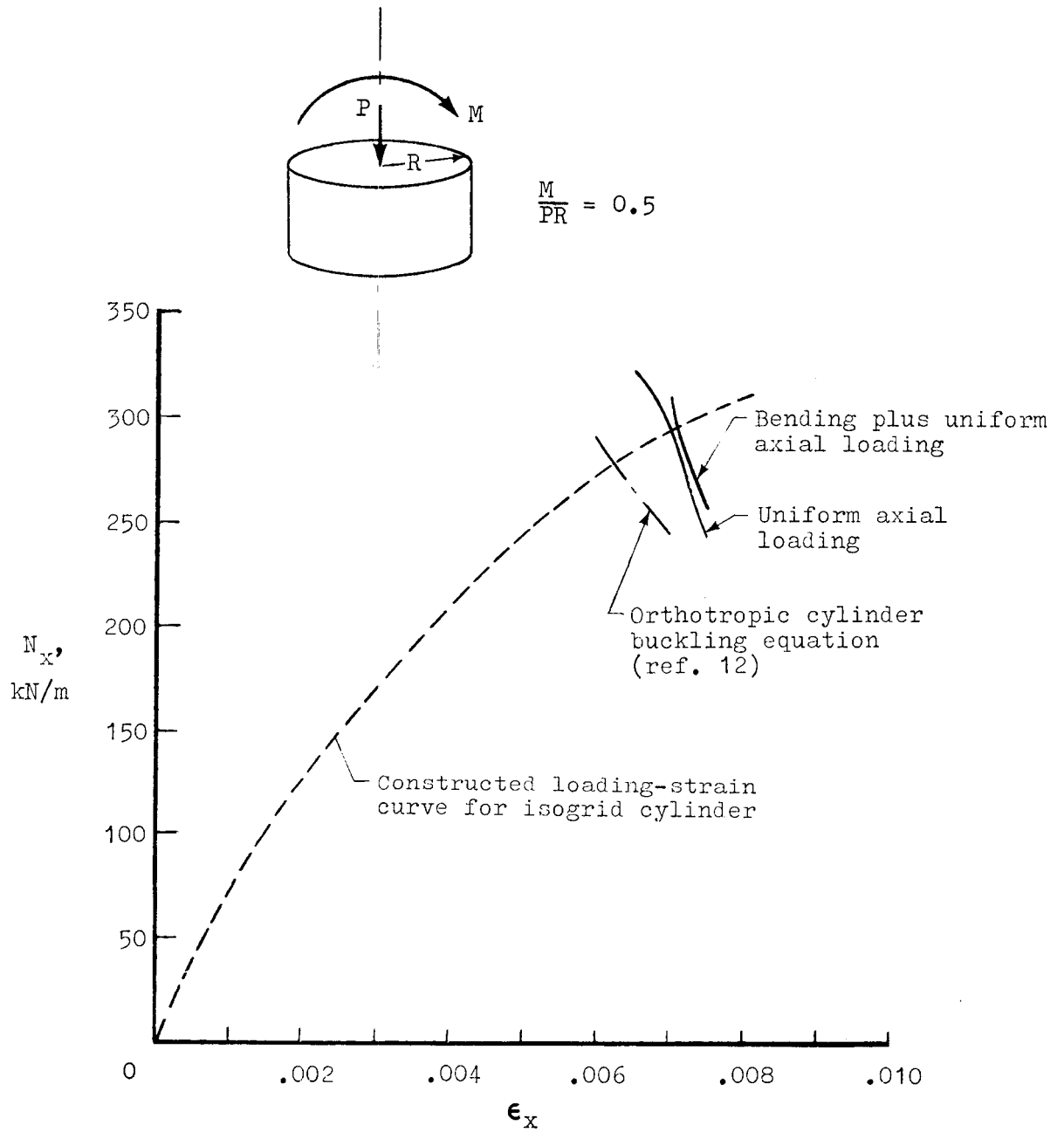

Figure 17.- Method for determining buckling load for strain above proportional limit.

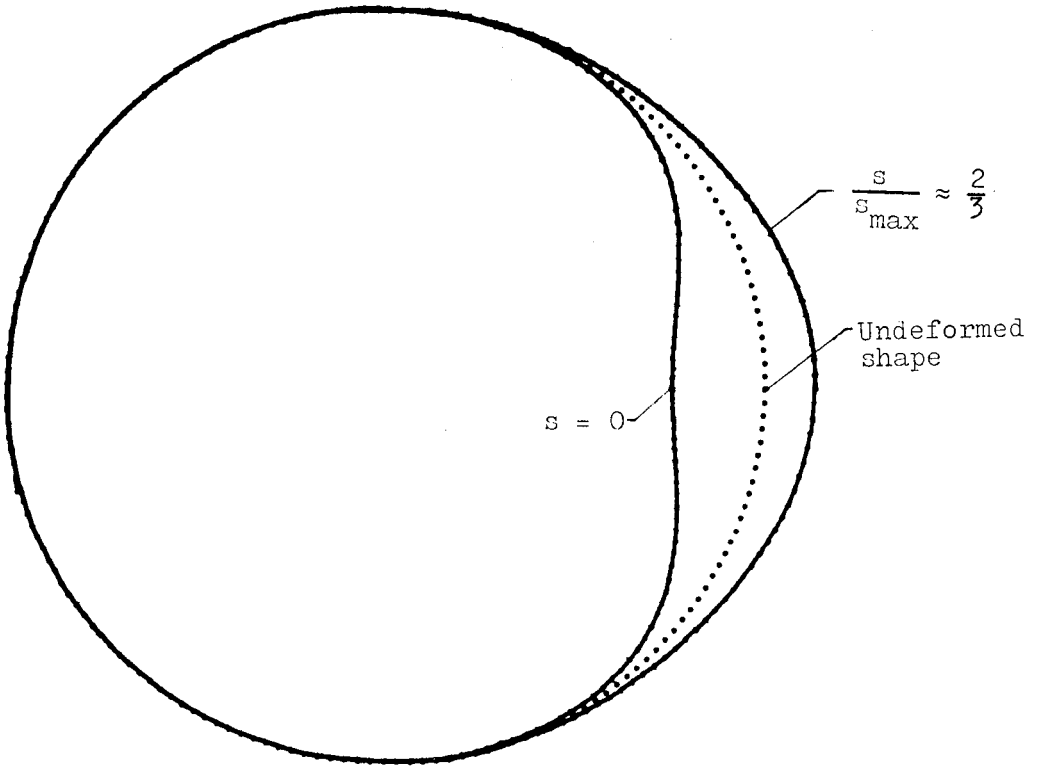

(a) Circumferential mode shape.

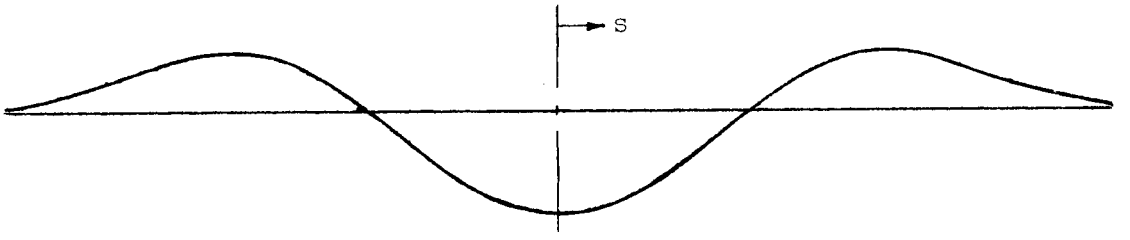

(b) Meridional mode shape.

Figure 18.- Buckle mode shape for uniform axial compressive loading plus bending. Symmetric conditions imposed at $s = 0$. Buckling $N_x = 292.1$ kN/m.

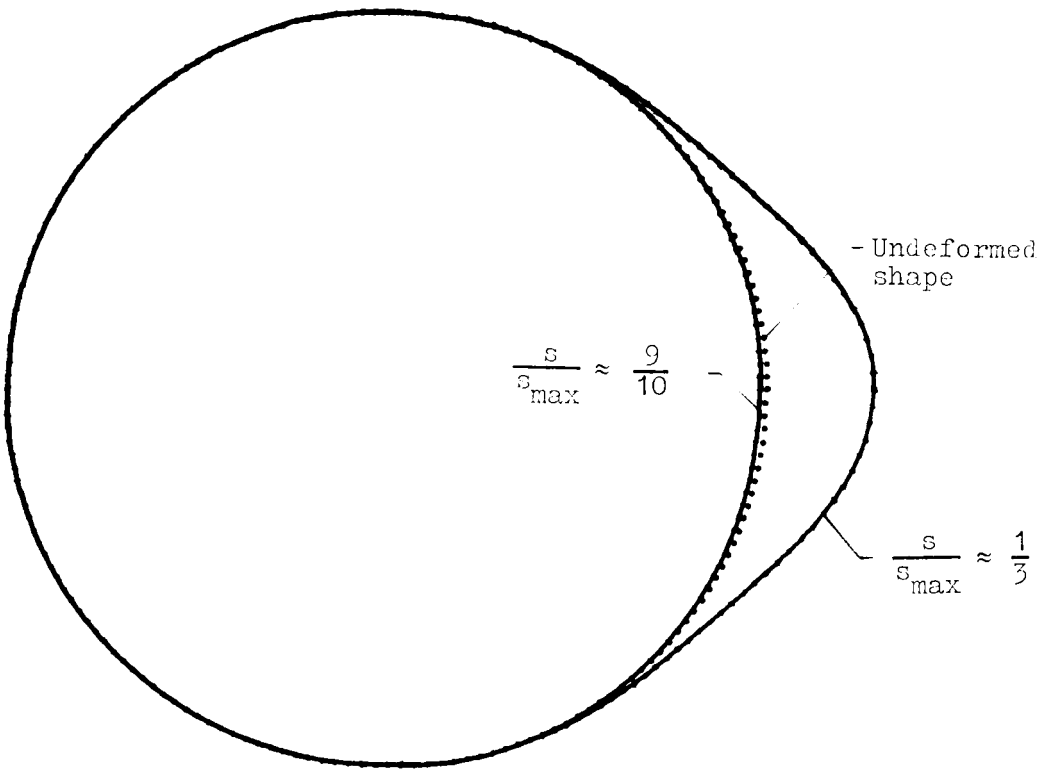

(a) Circumferential mode shape.

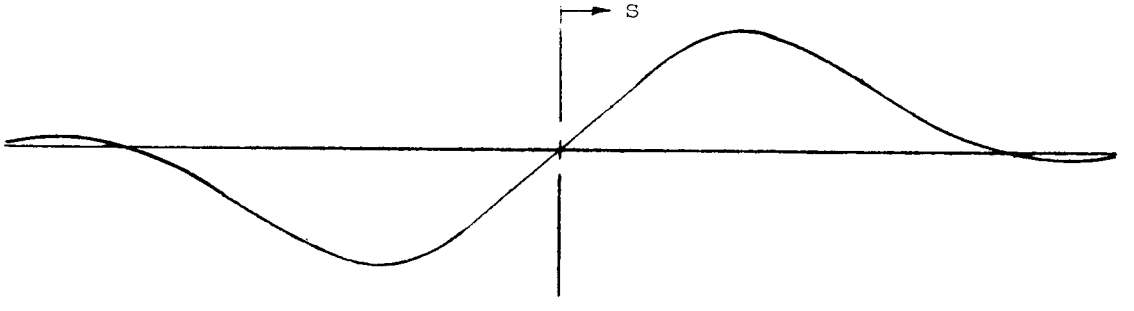

(b) Meridional mode shape.

Figure 19.- Buckle mode shape for uniform axial compressive loading plus bending. Antisymmetric conditions imposed at $s = 0$. Buckling $N_x = 295.6$ kN/m.

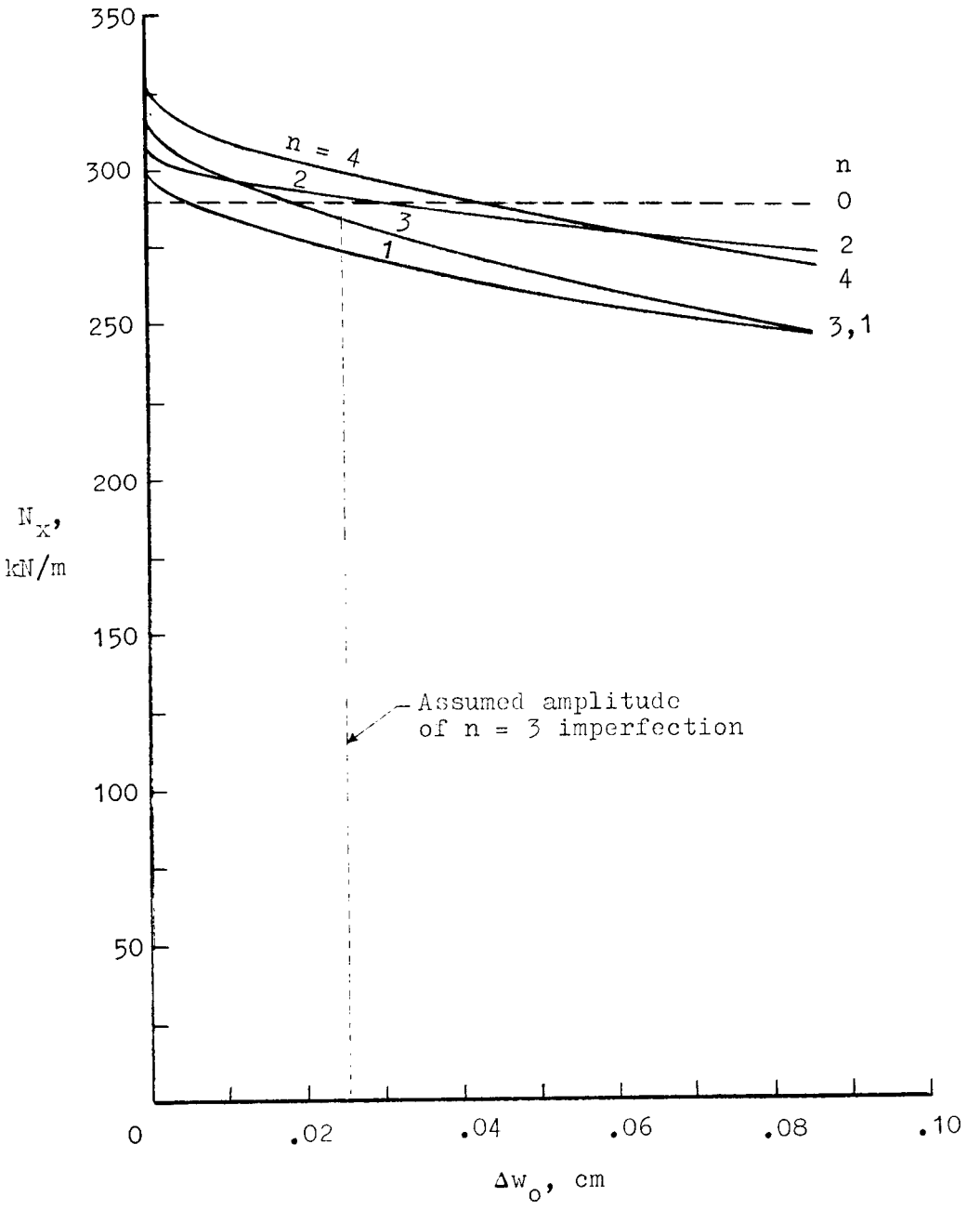

Figure 20.- Sensitivity of isogrid cylinder with meridional curvature loaded in uniform axial compression to initial imperfections having the same shape as the circumferential buckling mode. (Maximum measured Δw_o = 0.076 cm.)

1. Report No.	2. Government Accession No.	3. Recipient's Catalog No.
NASA TN D-8239		

4. Title and Subtitle	5. Report Date
AN ENGINEERING PROCEDURE FOR CALCULATING COMPRESSIVE STRENGTH OF ISOGRID CYLINDRICAL SHELLS WITH BUCKLED SKIN	June 1976
	6. Performing Organization Code
7. Author(s)	8. Performing Organization Report No.
Walter L. Heard, Jr., Melvin S. Anderson, and Paul Slysh	L-10860
	10. Work Unit No.
9. Performing Organization Name and Address	506-17-25-01
NASA Langley Research Center Hampton, Va. 23665	11. Contract or Grant No.
	13. Type of Report and Period Covered
12. Sponsoring Agency Name and Address	Technical Note
National Aeronautics and Space Administration Washington, D.C. 20546	14. Sponsoring Agency Code

15. Supplementary Notes

Paul Slysh: General Dynamics Corporation, Convair Division, San Diego, California.

16. Abstract

An engineering procedure is presented for calculating the compressive buckling strength of isogrid cylinders using shell-of-revolution techniques and accounting for loading beyond the material proportional limit and/or local buckling of the skin prior to general buckling. A general nondimensional chart (based on a nonlinear postbuckling analysis of a typical skin element) is presented which can be used in conjunction with formulas based on simple deformation plasticity theory to calculate postbuckling stiffnesses of the skin. The stiffening grid system is treated as an equivalent isotropic grid layer. Stiffnesses are determined for this grid layer, when loaded beyond the proportional limit, by the same plasticity theory used for the skin and a nonlinear stress-strain curve constructed from simple isogrid-handbook formulas and standard-reference-manual stress-strain curves for the material involved. Comparison of prebuckling strains and buckling results obtained by this procedure with data from a large isogrid-cylinder test is excellent with the calculated buckling load no more than 4 percent greater than the test value.

17. Key Words (Suggested by Author(s))	18. Distribution Statement
Cylinder buckling Isogrid cylinders Shell buckling	Unclassified – Unlimited Subject Category 39

19. Security Classif. (of this report)	20. Security Classif. (of this page)	21. No. of Pages	22. Price*
Unclassified	Unclassified	36	$3.75

*For sale by the National Technical Information Service, Springfield, Virginia 22161